UNIVERSITÀ DI PISA
UNIVERSITÀ DI PISA

FACOLTÀ DI SCIENZE MATEMATICHE, FISICHE E NATURALI
Corso di Laurea Specialistica in Scienze Fisiche
Anno Accademico 2010/2011

Tesi di Laurea Specialistica

Low Emittance Studies for a High Luminosity B-factory (SuperB)

Presentata da:
Simone Maria Liuzzo

Relatore:
Prof. Franco Cervelli

Correlatori:
Dott.sa Maria Enrica Biagini
Prof. Pantaleo Raimondi

to my grandmothers
Neva and Minnie

CONTENTS

OBJECTIVES

> "...it has been proven that Chess Masters concentrate on the weak points of a move, while beginners concentrate to verify their hypothesis instead of falsifying it..."
>
> N. N. Taleb
> *The Black Swan*

The *SuperB* Factory project aims at the construction of a high luminosity, two rings, asymmetric e^+e^- collider at the center of mass energy of the $\Upsilon(4S)$ resonance. The two beams will be stored in a 6.7 GeV High Energy Ring (HER) and a 4.2 GeV Low Energy Ring (LER). This project differs from the previous B-Factories, PEP-II [1] operating at SLAC (US) and KEKB [2] at KEK (Japan), for the very high design luminosity of $10^{36}\,cm^{-2}s^{-1}$, two orders of magnitude higher that the maximum ever reached at this energy. For this reason, the SuperB design concepts are not based on the conventional "high currents and short bunches" approach used in the past accelerators, but will allow reaching such a high events rate production thanks to a new collision scheme - the so called "large Piwinski angle and crab waist", - which has been originally developed by P. Raimondi at the Frascati National Laboratories, and successfully tested there on the DAΦNE Φ-factory [3]. One of the ingredients of this scheme is the extremely low beam emittances required: in particular the vertical one is comparable to those achieved in the latest generation Synchrotron Light Sources, such as DIAMOND at RAL (UK)[4] and Swiss Light Source at PSI [5] (Switzerland). With respect to these accelerators SuperB has the complication of a Final Focus insertion where the beams will be focused to extremely low beam sizes for the beam-beam collision, with consequent expected distruption of the emittance values. For this reason it is very important to study the impact of a "real" distribution of machine imperfections on the "design" emittance, simulating magnets errors, like misalignments and tilts, as well as possible errors in the Beam Position Monitors (BPM) that are used to measure the beam orbit.

The aim of this study is not only to check that such ultra low emittances can actually be reached, and the unavoidable machine errors will not have an impact on the luminosity performances, but also to determine a Table of Tolerances for magnet errors which will be used for the machine construction. It is then crucial to study the influence of such errors on the "real" emittances, by simulating the behavior of the accelerator under different error conditions and to study a procedure (so called "Low Emittance Tuning") to maintain the emittances at the design values. In the work presented here different errors and correction elements distributions have been considered, as well as different techniques to calculate the correction kicks to achieve the design emittances, which for SuperB are 5 pm (HER) and 6 pm (LER) for the vertical plane, and 2 nm (HER) and 2.5 nm (LER) for the horizontal one.

Low Emittance Tuning

In this thesis the work done on the simulation of how relevant beam parameters, such as emittances, closed orbit amplitude, vertical dispersion, β-beating and beam coupling vary under realistic conditions of magnets errors, like misalignments and tilts, will be presented. This study is focused for simplicity on the High Energy Ring, excluding the Final Focus (FF) insertion. This choice does not limit the results obtained, since the FF region is usually aligned with much more care than the rest of the machine, due to the presence of critical elements such as the final quadrupole doublets, with extremely high gradients, used to focus the beams at the Interaction Point (IP). Moreover the tools developed for this thesis can be easily extended to the study of the FF tolerances, work that will be performed in the near future. The application to a simpler machine layout has been chosen in order to check the capabilities of this procedure developed "ad hoc". Different machine corrections scheme have been studied to determine the most economic, in terms of corrector strengths, and effective way to achieve the needed beam parameters. The analysis has been performed with different distributions of correctors and BPM, and developing different "kicks" calculation techniques.

A particular feature of the work presented here is the development of a new method for orbit steering to correct at the same time effects such as betatron coupling and β-beating, without the insertion of new magnetic elements like "skew quadrupoles", as usually done in other storage rings. This technique was applied at LEP (CERN) [6] in the past, but never systematically used, and no automatic tool was ever developed, such as the one presented here. The novelty of the method is the use of the machine magnets itself as correcting elements, implemented by selecting

Betatron coupling and β-beating correction

the orbit that generates the minimum distortions and consequently the minimum emittance growth.

Table of Tolerances

The final outcome of this work is the Table of Tolerances with the maximum error sets which can be tolerated in the SuperB accelerator without loss in luminosity. The table is obtained through an optimization of the correctors and monitors layout and by means of the new orbit-coupling-dispersion correction scheme.

Even if this study has been focused on SuperB, however its application to other storage rings is straightforward, since the software has been developed together with a particularly flexible and user friendly graphic interface, able to deal with all the steps involved in the optimization procedure. This work will continue to implement the study of tolerances for the critical Final Focus section, as well as for the SuperB Low Energy Ring, and its results will be part of the SuperB Technical Design Report to be published in 2011. It is also foreseen the application of the procedure described in this thesis to an existing storage ring, the DIAMOND synchrotron light source, where its efficacy will be tested on a real beam.

In Chapter 1 the SuperB project will be briefly described, with focus on the accelerator characteristics. In Chapter 2 a description of the Low Emittance Tuning concept and of the possible magnets errors will be given. Chapter 3 will describe the tool expressly developed for this thesis and the results of the study are described in Chapter 4. Conclusions are in Chapter 5, while in the Appendix short descriptions of the main physics and machine concepts used in this work are reported.

1 SUPERB

The paragraphs below summarize the SuperB Factory project, the Physics motivations and the accelerator design. For a complete reference see [7, 8, 9, 10].

1.1 PHYSICS

The *Standard Model* (SM) is the most advanced and confirmed theory up to today to explain the fundamental interactions of particles. The search for new phenomena violating or confirming this model, like the evidence for the existence of the Higgs boson, is now taking place at large experiments as the LHC [11]. High statistics studies of heavy quarks and leptons will have a crucial role to play in the field of SM violations.

New particles can reveal themselves through loops effects in decays of Standard Model particles such as B and D mesons and τ leptons. Since quantum effects typically become smaller as the mass of the virtual particles increases, high-precision measurements are required to have an extended mass reach. In some instances, in fact, high-precision measurements of heavy flavor decays allow us to probe New Physics energy scales inaccessible at present and next-generation colliders. Flavor physics is fertile ground for New Physics searches for several reasons.

Flavor Changing Neutral Currents (FCNC), neutral meson-antimeson mixing and CP violation occur only at the loop level in the Standard Model and are therefore potentially subject to $\mathcal{O}(1)$ New Physics virtual corrections. In addition, quark flavor violation in the Standard Model is governed by the weak interaction and suppressed by the small Cabibbo-Kobayashi-Maskawa (CKM) mixing angles. These features are not necessarily shared by New Physics, which could, therefore, produce very large discrepancy from the standard model prediction in particular cases.

These searches in the heavy flavor Physics sector are the motivation of the construction of a Super-B Factory, the next generation asymmetric e^+e^- flavor factory with a peak luminosity of $10^{36}\mathrm{cm}^{-2}\mathrm{s}^{-1}$. This factory is designed to work at the $\Upsilon(4S)$ Center of Mass energy, producing a

sample of $75\,ab^{-1}$ $B\bar{B}$ events, 100 times that of previous experiments like BABAR [12] and Belle [13]. To show the capability of this high luminosity factory a selection of measurements that will be possible at SuperB is discussed in more detail following [9].

Rare B decays

The most appealing decays to evidence SM discrepancy are those with a low SM uncertainty that may be described by other New Physics (NP) models. These golden channels are for a large fraction decays of B mesons with a very small branching ratio. Some of these decays are reported in Table 1.1.

		sensitivity	
observable	NP Scenario	current	SuperB ($75\,ab^{-1}$)
$\mathcal{B}(B \to X_s\gamma)$	Minimal FV	7%	3%
$\mathcal{A}_{CP}(B \to X_s\gamma)$	Non-Minimal FV	0.037	$0.004 - 0.005$
$\mathcal{B}(B \to \tau\nu)$	H^+ high $\tan\beta$	30%	$3 - 4\%$
$\mathcal{B}(B \to K\nu\bar{\nu})$	Z-penguins	-	$16 - 20\%$
$\mathcal{B}(\tau \to \mu\gamma)$	LFV	$4.5\,10^{-8}$	$2\,10^{-9}$
$\mathcal{B}(\tau \to e\gamma)$	LFV	$1.1\,10^{-7}$	$2\,10^{-9}$

Table 1.1: Rare B decays (FV = Flavor Violation)

These decays are specific of SuperB since at hadronic colliders those events are not reconstructible and even at SuperB they are not of easy detection. Compared to other lepton colliders, the accuracy on these measurements may be increased significantly compared to that of previous experiments as it is shown in Table 1.1.

With these decays it may also be possible to give better constraints on quantities of great interest like the Higgs boson mass. For example in a scenario with high $\tan\beta$ the decay $B \to \nu\tau$ is strongly affected by the presence of charged Higgs. The contribution to the amplitude, considering a scalar Higgs field, would be

$$(1 - \tan^2\beta(\frac{M_B^2}{M_{H^+}^2}))^2$$

where M is the mass of the particles and β the unitarity triangle angle (see A.2). Measurement of the branching ratio of this decay with $75\,ab^{-1}$,

given a hypothetical value of $\tan\beta = 50$, may constrain the Higgs mass lower bound to the level of the $\simeq 2\text{TeV}$ improving consistently the actual bound around 1GeV.

Time Dependent CP Asymmetries

Another antenna for the presence of NP is given by time dependent asymmetries [14] in penguin dominated B decay modes. Penguins are one loop contribution to decays where one of the two b quark converts in a s quark with a one loop diagram as shown in Figure 1.1. In the

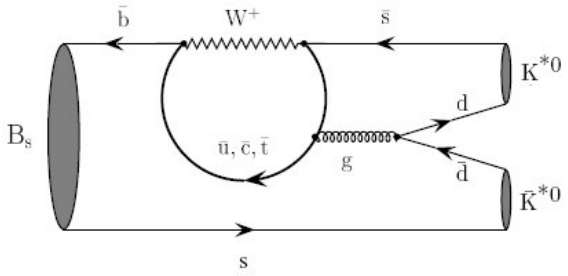

Figure 1.1: Feynman diagram of $B \to K^{0*}\bar{K^0}^*$ decay, as an example of penguin diagram

SM the time dependent asymmetries are a direct measure of the angle $\sin 2\beta$ and are determined to very high order. This leads to a very accurate measurement so that the difference between the measurement with penguins and without them should be equal giving

$$\Delta S = \sin 2\beta|_{b\to s} - \sin 2\beta \simeq 0.$$

The presence of NP particles in the penguins would generate measurable deviations from zero. The accuracy reached on the measurement of $\sin 2\beta|_{b\to s}$ is a key parameter that can be improved consistently at SuperB, observing decays like $B \to K_s K_s K_s$, $B \to \eta' K^0$ and $B \to \phi K^0$ sensible probes for NP. The measurements involving time dependence require a boost in the CM to determine the direction of motion and so the time of decay by the length of the path between particle generation and the point of the decay. For this reason an asymmetric collider is needed together with a high precision tracking detector like SVT [15].

CKM Parameters

A very strong check for the presence of NP is to verify that the unitary triangle (see A.2) is indeed a triangle. To measure the angles α, β and γ the following decays (and similar) are studied:

$$B_d^0 \rightarrow J/\Psi K_s \text{ for } \sin 2\beta, \tag{1.1}$$
$$B_d^0 \rightarrow \pi^+\pi^- \text{ for } \sin 2\alpha, \tag{1.2}$$
$$B_s^0 \rightarrow D_s^{\pm}K^{\mp} \text{ for } \sin 2\gamma. \tag{1.3}$$

With SuperB a very high precision may be reached in these measurements, improving of a factor 10 the actual bounds. As shown in Figure 1.2, where for the same central values, actual errors and SuperB expected errors are compared: if no consistency is found in the $\bar{\rho} - \bar{\eta}$ plane (no overlap of the colored sections), than a new explanation will be needed, to give sense to the non unitarity of the CKM matrix (see Appendix).

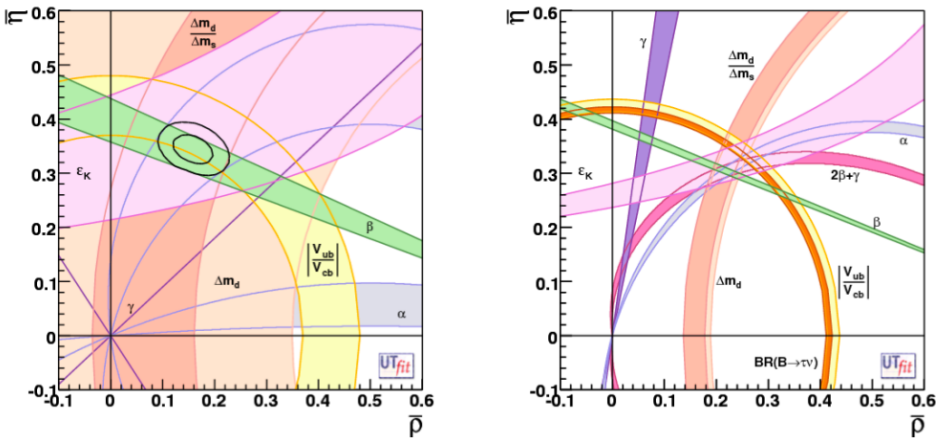

Figure 1.2: Unitary Triangle Fit

Lepton Flavor Violation (LFV)

In the SM, lepton families are not mixing like quark families do for weak interactions. The observation of a lepton flavor violation in τ decays like

$$\tau \rightarrow \mu\gamma$$

,

$$\tau \rightarrow e\gamma$$

would be an other clear evidence of NP, and SuperB will be able to study those decays. Compared to current B-factories the great amount of data collected by SuperB will be able to increase the sensitivity of a factor 7. Moreover SuperB electron beam will be polarized leading to a consistent improvement in signal separations and if LFV is observed will give more informations about its features.

Charm Physics

SuperB is designed to operate at different energies in different upgrades and it will work also as a charmed meson factory with CM energies of $\Upsilon(4S)$ and $\Psi(3770)$. The cross section for $c\bar{c}$ production $\sigma(e^+e^- \rightarrow c\ \bar{c}) \sim 1.3\,nb$ is similar to that of $b\bar{b}$, but since the energy is lower, luminosity decreases of a factor 10. At this CM energy observation of $D^0 - \bar{D}^0$ oscillations is the most appealing probe for CP violation, but also rare decays are available for study at this energy and CKM matrix elements may still be studied. On the Unitary triangle there is no improvement since the triangle that involves charm decays is highly degenerate.

1.2 ACCELERATOR

The experiments described above require to study events with very low cross sections. Good statistics and so high precision can be achieved only if high rates of events are produced. Rate R of events produced at the interaction point and event cross section σ are related by

$$R = \mathcal{L}\sigma \tag{1.4}$$

where $\mathcal{L}$ is the machine *Luminosity*. To increase the rates high luminosity is required. The luminosity for a e^+e^- collider, when beams cross in the horizontal plane with an angle θ may be written as [1]:

$$\mathcal{L} = \frac{N^+N^-}{4\pi\sigma_y\sqrt{(\sigma_z \tan\frac{\theta}{2})^2 + \sigma_x^2}} f_c \tag{1.5}$$

with

$$\sigma_{x,y} = \sqrt{\beta_{x,y}\epsilon_{x,y}} \tag{1.6}$$

where f_c is the collision frequency, N^+ and N^- are the number of particles in the positron and electron bunches, $\sigma_{x,y,z}$ are the beam rms sizes in the horizontal, vertical and longitudinal directions, $\epsilon_{x,y}$ are the beam emittances, $\beta_{x,y}$ are the beta functions (in cm) at the collision point in each plane and θ is the crossing angle between the beams at the interaction point (IP).

Very important in SuperB design is to keep beam currents and bunch length at the same level of actual B-factories, while increasing the luminosity, in order to keep power consumption under control. The key issues for this design are: crab waist scheme and low emittance. A specifically designed lattice can reach very low vertical emittance and consequently high luminosity, that may be further increased by the crab waist collision scheme to reach $10^{36}\,cm^{-2}s^{-2}$ (a factor 100 higher than the luminosity of today working colliders). The specification of this design will be further explained in the following sections. From the point of view of low emittance, SuperB can be considered as a "Damping Ring" similar to those designed for the Linear Colliders such as CLIC and ILC, with the complication of a sophisticated Final Focus section to obtain high Luminosity.

High Luminosity: $10^{36}\,cm^{-2}s^{-2}$

As for other B-factories, the energy of the two rings are different to allow the necessary boost for the decayed particles: the High Energy

1 assuming a NON asymmetric collider

Ring (HER) produces 6.7 GeV positrons, while the Low Energy Ring (LER) provides 4.18 GeV electrons. In Figure 1.3, the layout of the two rings is shown in one of the proposed sites, i.e. the National Laboratory of Frascati (LNF), Italy.

Figure 1.3: SuperB at the Frascati site

1.2.1 High Luminosity

In present and future colliders different methods have been used to achieve high luminosity [16].

Conventional methods

All the present high luminosity factories relied, at least at the beginning of their operation, on standard strategy of choosing beam parameters to achieve high luminosity, strategy that is summarized in the following. According to the expressions for the luminosity L written as a function of beam-beam tune shifts $\xi_{x,y}$:

$$\mathcal{L} = N_b f_0 \frac{N^2}{4\pi\sigma_y^*\sigma_x^*} \tag{1.7}$$
$$= N_b f_0 \frac{\pi\gamma^2 \xi_x \xi_y \epsilon_x}{r_e^2 \beta_y^*}(1 + \frac{\sigma_y^*}{\sigma_x^*})^2$$

$$\xi_{x,y} = \frac{r_e N}{2\pi\gamma} \frac{\beta_{x,y}^*}{\sigma_{x,y}^*(\sigma_x^* + \sigma_y^*)} \tag{1.8}$$

(where γ is the lorenz factor, N_b the number of bunches, f_0 the revolution frequency, N the number of particles per bunch, r_e the classical electron radius and * indicates quantities calculated at the IP) at a given energy the key requirements to increase the luminosity are:

- Higher number of particles per bunch N
- More colliding bunches N_b
- Larger beam horizontal emittance
- Smaller beta functions at the interaction point (IP)
- Round beams $\sigma_x^* = \sigma_y^*$ [2]
- Higher tune shift parameters.

The present factories have obtained their good luminosity performances trying to fulfill almost all the above conditions as much as possible, a part the use of flat bunches ($\sigma_x^* \ll \sigma_y^*$) as it is rather difficult to provide a good dynamic aperture for the round beam case with low beta functions both in vertical and in horizontal plane at the IP. Besides, in order to eliminate parasitic collisions (PC), i.e. collision points before and after the IP, in multibunch operation, a small horizontal crossing angle was necessary. In the factories a relatively small Piwinski angle

$$\varphi = \frac{\sigma_z}{\sigma_x} \tan\frac{\theta}{2} < 1 \tag{1.9}$$

2 This technique is not evident from the formulas above. It requires $\beta_x = \beta_y$, $\epsilon_x = \epsilon_y$ and $\nu_x = \nu_y$. The rotational symmetry of the kick from the round opposite beam, complemented with the X-Y symmetry of the betatron transfer matrix between the collisions, result in an additional integral of motion $M = xy' - yx'$, i.e. the longitudinal component of particle's angular momentum. Thus, the transverse motion becomes equivalent to a one-dimensional motion, with the resulting elimination of all betatron coupling resonances [17]. In terms of luminosity the gain is due to the possible strong enhancement of the horizontal tune shift due to the absence of this resonances.

was mandatory to avoid excessive geometric luminosity reduction and to diminish the strength of synchrobetatron resonances arising from beam-beam interaction with the crossing angle (see Appendix).

A further substantial luminosity increase based on the "standard collision scheme" is proposed for SuperKEKB B-Factory in Japan: it relies on pushing currents to unprecedented values (ex. 9A) and on shortening the bunches (3 mm). Such approach may result to be hardly possible, due to several limitations such as: 1) an increase of the high order modes in the beam pipe (with consequent raise of beam instabilities), 2) increase of cavity voltage and higher power consumption due to the very high currents.

However, the very short bunch length allows to have lower β_y^*. Since the β functions have a waist at the Interaction Point (IP) and a parabolic behavior (see Figure 1.4), due to the finite beam longitudinal distribution, particles in the tails of the beam "see" a much higher β_y^*. As a consequence the achievable luminosity is reduced. This effect is called *"Hourglass Effect"* (see Appendix) and empirically the requirement to minimize it is $\beta_y^* > 2\sigma_z$.

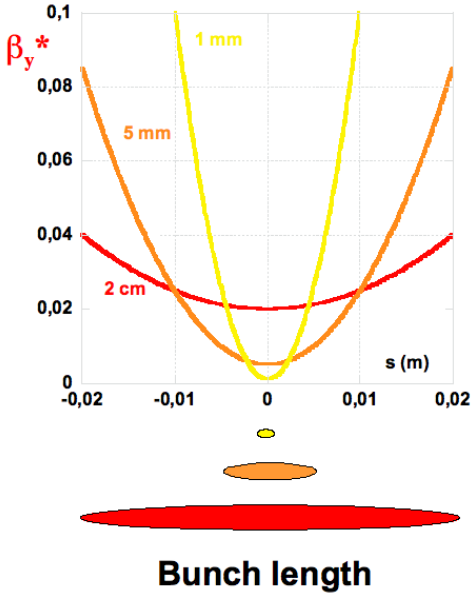

Figure 1.4: Bunch length and β functions at the IP

In order to overcome these limitations several novel collision concepts and new collision schemes have been proposed, such as: round beam collision preserving an additional integral of motion [17]; crab crossing

[18, 19]; collision with large Piwinski angle [20]; longitudinal strong RF focusing [21] ; collision with traveling waist [22]; crab waist collision [23, 24]. This last scheme as been tested at DAΦNE and has been adopted for the SuperB factory for his promising qualities.

Large Piwinski Angle and Crab Waist

Contrary to the conventional strategy, the crab waist collision scheme (CW) requires small emittance ϵ_x and larger Piwinski crossing angle. In this scheme there is no need to decrease the bunch length and push beam currents far beyond the values already achieved in the present factories. The CW can substantially increase collider luminosity thanks to several potentially advantageous ideas: collisions with a large Piwinski angle, micro-beta insertions and suppression of beam-beam resonances using the dedicated ("crab waist") sextupoles.

The advantages became clear when considering two bunches colliding under a horizontal crossing angle (as shown in Figure 1.5).

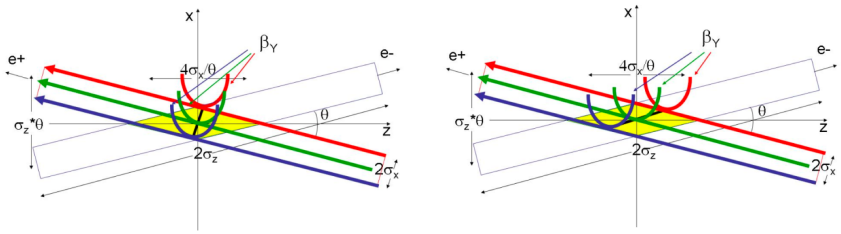

Figure 1.5: CrabWaist sextupoles off (left) and on (rigth)

In this configuration the CW principle can be seen, somewhat artificially, as a process with three basic steps. The first one is large Piwinski angle. For collisions with $\varphi \gg 1$ (see 1.9) the luminosity L and the beam-beam tune shifts scale as (see, [25]):

Large Piwinski Angle

$$\mathcal{L} \propto \frac{N\xi_y}{\beta_y^*}; \tag{1.10}$$

$$\xi_y \propto \frac{N\sqrt{\beta_y^*}}{\sigma_x\sqrt{1+\varphi^2}} \simeq \frac{2N\sqrt{\beta_y^*}}{\sigma_z\theta}; \tag{1.11}$$

$$\xi_x \propto \frac{N}{\sigma_x^2(1+\varphi^2)} \simeq \frac{4N}{(\sigma_z\theta)^2} \tag{1.12}$$

In such a case, if it were possible to increase N proportionally to $\sigma_z\theta$, the vertical tune shift ξ_y would remain constant, while the luminosity

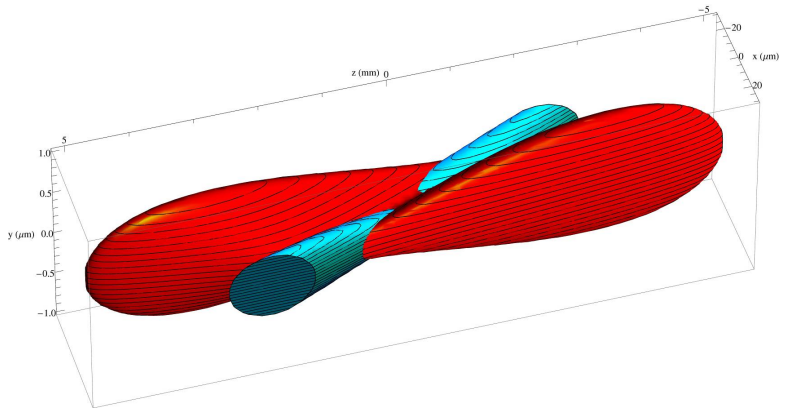

Figure 1.6: Effect of the Crab Waist Collision scheme

would grow proportionally to $\sigma_z\theta$. Moreover, the horizontal tune shift would drop as $\frac{1}{\sigma_z\theta}$ increasing beam stability. Differently from previous colliders, in the crab waist scheme the Piwinski angle is increased by decreasing the horizontal beam size σ_x and increasing the crossing angle θ. In this way it is possible to gain in luminosity as well, and the horizontal tune shift decreases. Moreover, parasitic collisions become negligible since with higher crossing angle and smaller horizontal beam size the beam separation at the PC is large in terms of σ_x. But the most important effect is that the length of the overlap area of the colliding bunches is reduced, since it is proportional to $\frac{\sigma_x}{\theta}$ (see Figure 1.5).

Then second step consists in requiring the vertical beta function β_y be comparable to the overlap area size (i.e. much smaller than the bunch length, but avoiding Hourglass effect):

$$\beta_y \simeq \frac{2\sigma_x}{\theta} \simeq \frac{\sigma_z}{\varphi} << \sigma_z.$$

So, reducing β_y at the IP gives us several advantages:

- Luminosity increase with the same bunch current.
- Possibility of the bunch current increase (if it is limited by ξ_y), thus further increasing the luminosity.
- Suppression of the vertical synchrobetatron resonances.
- Reduction of the vertical tune shift.

Besides, there are additional advantages in such a collision scheme: there is no need to decrease the bunch length to increase the luminosity, as proposed in standard upgrade plans for B- and Φ-factories.

This will help in solving the problems of High Order Mode (HOM) heating[3], coherent synchrotron radiation of short bunches, excessive power consumption, etc.

Crab Waist

However, implementation of these two steps introduces new beam-beam resonances which may strongly limit the maximum achievable tune shifts. The crab waist scheme avoids this problems, so boosting the luminosity: this represents the third step. As it can be seen in Figures 1.5 and 1.6, the beta function waist of one beam is oriented along the central trajectory of the other one. In practice the CW vertical beta function rotation is obtained by means of sextupole magnets placed on both sides of the IP, in phase with the IP in the horizontal plane and at $\pi/2$ in the vertical one. The crab sextupole strength K is required to fulfill the following condition:

$$K = \frac{1}{\theta}\frac{1}{\beta_y^* \beta_y}\sqrt{\frac{\beta_x^*}{\beta_x}} \tag{1.13}$$

In the 1.13 the K depends on the crossing angle, the beta functions at the IP and on the sextupole locations. The crab waist transformation provides a small geometric luminosity gain due to the vertical beta function redistribution along the overlap area: this gain is estimated to be of the order of several percent. However, the dominating effect consists on the suppression of betatron (and synchrobetatron) resonances always present in collisions without CW due to the coupling of horizontal, vertical and longitudinal motion. Figure 1.7 demonstrates the resonances suppression, showing the luminosity in tune space with CW sextupoles off (left) and on (right) [27].

This new approach as been tested at the DAΦNE Φ-factory in Frascati. A gain in luminosity of a factor of ~ 3 with respect to the previous records [3] was obtained (Figure 1.8) and in complete agreement with simulations. In Figure 1.9 the luminosity obtained with and without the crab sextupoles are compared, evidencing the improvement given by this technique.

This CW scheme, that takes advantage of the large Piwinski angle, is adopted as the key idea to reach the target luminosity at SuperB. The other stringent requirement comes from the beam emittance that has to be very small and particularly small in the vertical plane.

3 beam energy losses due to the excitation in RF cavity of frequencies different from the fundamental frequency of the cavity [26].

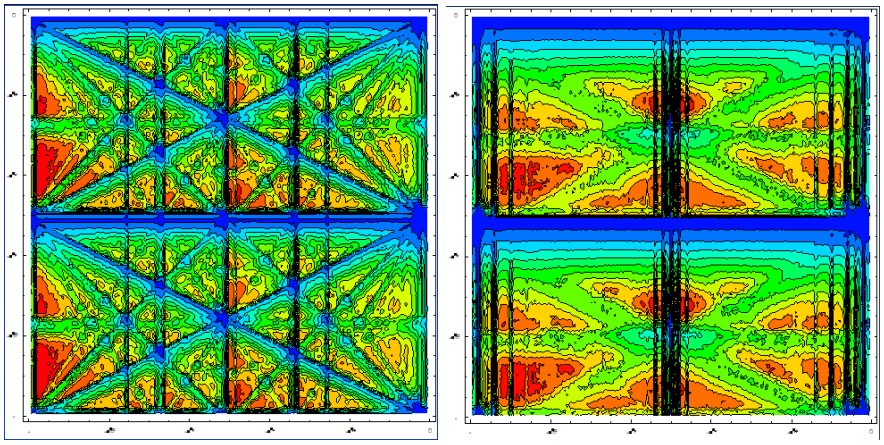

Figure 1.7: Effect of the Crab Waist Collision scheme in tune space. Crab OFF (left) and Crab ON (right). The wormer color indicate higher luminosity and the dark bands are the effect of resonances.

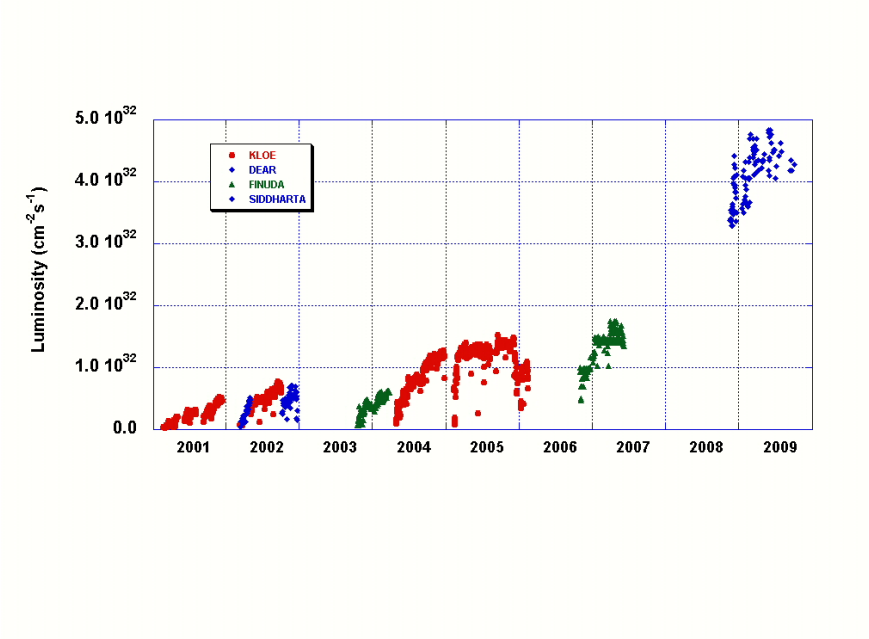

Figure 1.8: Luminosity at DAΦNE in the past years. The introduction of crab waist in 2008 gives an evident improvement in Luminosity.

Theoretically Minimum Emittance (TME) Lattice

In order to obtain the maximum luminosity the "large Piwinski angle and crab waist collision" scheme is required to be applied with a lattice as

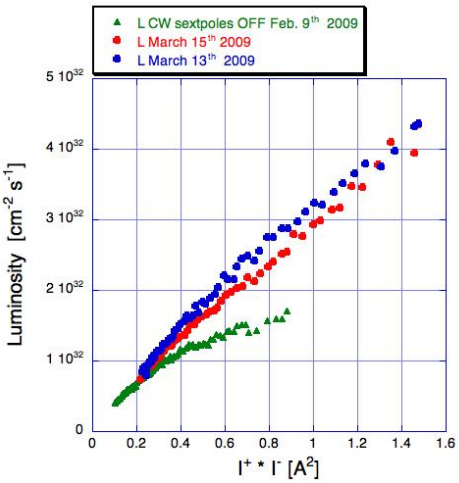

Figure 1.9: Luminosity versus beam current product at DAΦNE with crab waist on (blue) and crab waist off (red)

close as possible to the Theoretically Minimum Emittance Lattice (TME) (see equation 1.5). The emittance in the horizontal plane is determined by the equilibrium between synchrotron radiation damping and quantum excitation. This can be expressed by [28][29]

$$\epsilon_x^{TME} = C_q \gamma^2 \frac{I_5}{I_2 - I_4} \tag{1.14}$$
$$C_q = \frac{55\hbar}{32\sqrt{3} m_e c} = 3.8410^{-13} (mrad)$$

where γ is the Lorentz factor and the I's are the synchrotron radiation integrals

$$I_2[m^{-1}] = \oint \left(\frac{1}{\rho^2}\right) ds$$
$$I_4[m^{-1}] = \oint \frac{2D_x}{\rho^3} ds$$
$$I_5[m^{-1}] = \oint \frac{\gamma_x D_x^2 + 2\alpha_x D_x D_x' + \beta_x D_x'^2}{\rho^3} ds,$$

with ρ the local bending radius, D_x and D_x' the local dispersion and dispersion derivative and α_x and β_x the Twiss parameters (see Appendix).

In the vertical plane if there are no vertical bends the emittance is a reduced from of the previous equations, since only quantum effects are present.

$$\epsilon_y^{TME} = \frac{13}{55}\frac{C_q}{J_y I_2}\oint \frac{\beta_y}{\rho^3} ds \tag{1.15}$$

where J_y is the damping partition number in the y plane, and all quantities refer to the vertical plane (x subscripts became y).

The TME is the lattice that minimizes these two quantities. The minimum horizontal emittance is given by

$$\epsilon_x = \frac{C_q \gamma^2 \theta_b^3}{12\sqrt{15} J_x},$$

(J_x dumping partition number in the horizontal plane) which is achieved when $\alpha_x = D_x' = 0$, $\beta_x = \frac{L_b}{\sqrt{60}}$ and the dispersion $D_x = \frac{L_b \theta_b}{24}$ at the center of the dipoles with L_b and θ_b as length and bending angle. This last requirement evidences the importance of minimum dispersion in the bending magnet. Figure 1.10 shows a scheme that may be tuned to give these parameters.

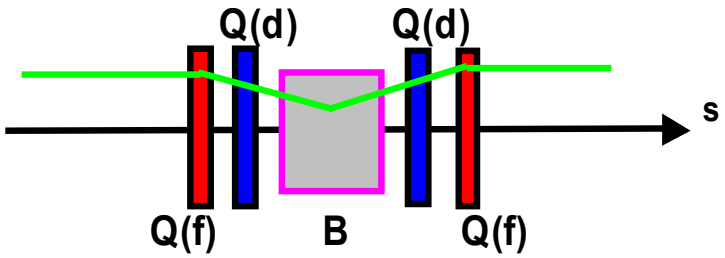

Figure 1.10: TME Lattice base design.[30]

The vertical emittance is very close to zero. However any misalignment error in the magnets, will result in a rise of the vertical emittance. The main source of this rise are the appearance of vertical kicks (see next chapter) and coupling due to the misalignments. This kick and couplings spoil the theoretical independence of the orbits in the two planes, moving part of the horizontal oscillation in the vertical plane and therefore, increase the vertical emittance. Since the emittances are very different and particularly, the vertical one is approximately zero,

these effects may be very large. In fact the influence of such errors introduced by magnet misalignments are the main topic of this thesis and will be simulated extensively.

1.2.2 SuperB Lattice

SuperB main components are the two storage rings: the Low Energy Ring, for electrons at 4.18 GeV, and the High Energy Ring for positrons at 6.7 GeV. SuperB lattice V12[31][32] layout is shown in Figure 1.11.

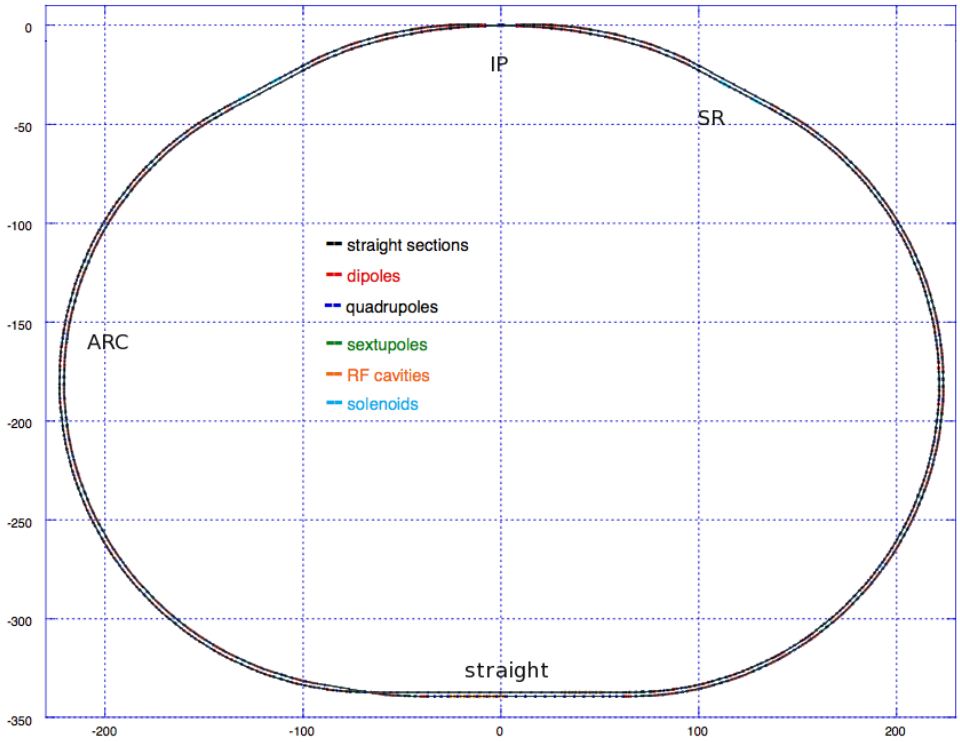

Figure 1.11: current SuperB V12 Lattice layout for HER and LER

Lattices for both rings are composed by two arcs and a Final Focus. A long straight section connects the arcs on the opposite side of Interaction Region. The straight section contains injection and Radio Frequency cavities and has space available for other instrumentations. The two rings are on the same plane and have approximately the same length (i.e.1258 m) but they are shifted so to be 2.1 m distant in the arcs. This allows ring separation in the tunnel, and two crossing points, one in the Final Focus for the Interaction Point and the other in the straight

section, lengthened slightly in the HER lattice to allow for the crossing without beam degradation.

A list of lattice and machine parameters is presented in Table 1.2.

Table 1.2: Preliminary parameters for SuperB

Parameter	Units	HER (e+)	LER (e-)
LUMINOSITY	$cm^{-2}\,s^{-1}$	1,00E+36	
Energy	GeV	6,7	4,18
Circumference	m	1258,4	
X-Angle (full)	mrad	66	
β_x @ IP	cm	2,6	3,2
β_y @ IP	cm	0,03	0,02
Coupling (full current)	%	0,25	0,25
Emittance x (with IBS)	nm	2,00	2,41
Emittance y	pm	5	5,8
Bunch length (full current)	mm	5	5
Beam current	mA	1892	2410
Tune shift x		0,0021	0,0033
Tune shift y		0,0978	0,0978
damping time Long.	msec	13,4	20,3
Touschek lifetime	min	35	16
Luminosity lifetime	min	4,82	6,14
Total lifetime	min	4,24	4,44
RF frequency	MHz	476	
Rev. frequency	Hz	2,38E+05	
Piwinski angle	rad	22,88	18,79
# of bunches	#	978	
N. Particle per bunch	#	5,08E+10	6,46E+10

Arcs

The lattice of the arcs is a modified Theoretical Minimum Emittance (TME) lattice. There are two different kinds of cells, characterized by the phase advance (μ) in the x plane: the short cell with $\mu_x = \frac{3}{2}\pi$ and $\mu_y = \frac{\pi}{2}$, shown in Figure 1.12(a) and the long cell, a double minimum emittance lattice, with $\mu_x = 3\pi$ and $\mu_y = \pi$, shown in Figure 1.12(c). The minimum β_x and horizontal dispersion in the bending magnets are also evidenced in Figures 1.12(b) and (d).

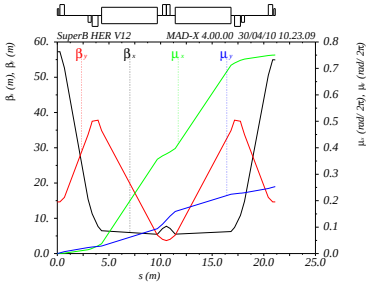

(a) *Short cell beta functions (β) and phase advance (μ).*

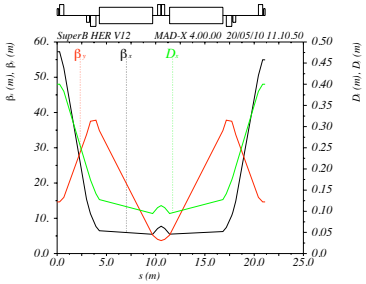

(b) *Long cell beta functions (β) and dispersion (D).*

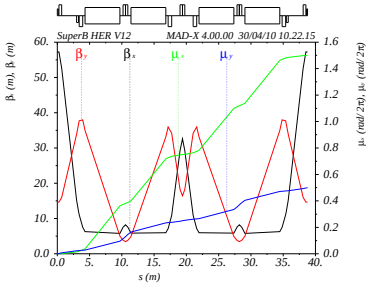

(c) *Long cell beta functions (β) and phase advance (μ) .*

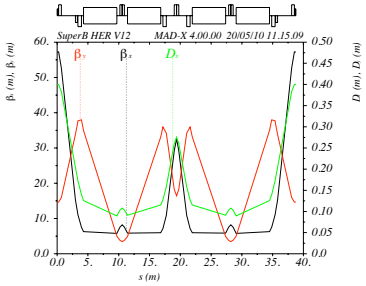

(d) *Long cell beta functions (β) and dispersion (D).*

Figure 1.12: Arc Cells for HER V12

The main difference of the cells from a TME is represented by the splitting of the central dipole into two parts to allow the insertion of an additional focusing quadrupole, so ensuring a better tunability of the cell.

One arc is composed of six of these cell couples, alternating a long and a short cell. This highly periodic lattice helps significantly to amplify

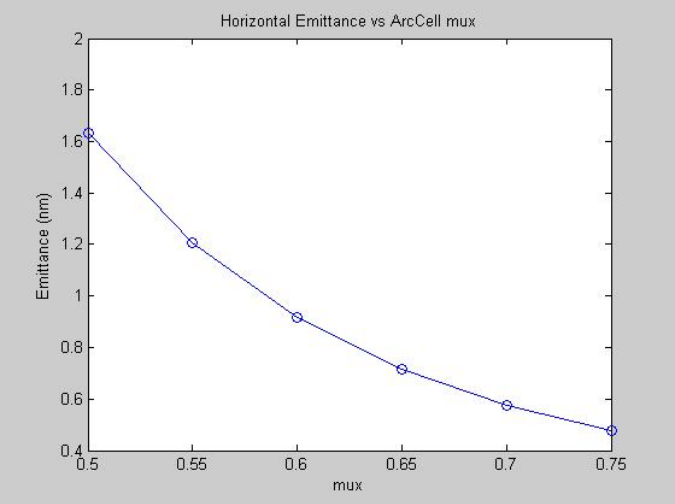

Figure 1.13: Horizontal emittance versus cell phase advance in the horizontal plane (μ_x).

the available tune space, allowing for a large variation of the tunes during operation for luminosity optimization.

The choice of a high phase advance is the result of the study shown in Figure 1.13: when the phase advance in the cell is increased the horizontal emittance decreases. Anyway a trade off has to be found with dynamic aperture, that decreases, due to the chromatic effects introduced by the high phase advance. The strong chromatic effects generated are compensated introducing strong sextupoles at the beginning and end of every cell where beta functions and dispersion are at maximum. In the next sections it will be shown how it is possible to take advantage of this sextupoles for orbit correction. The transport matrix of the long cell is exactly

$$-\mathcal{I} = \begin{pmatrix} -1 & 0 & 0 & 0 \\ 0 & -1 & 0 & 0 \\ 0 & 0 & -1 & 0 \\ 0 & 0 & 0 & -1 \end{pmatrix} \tag{1.16}$$

so that the identical sextupoles form $-\mathcal{I}$ pairs which provide local cancellation of the sextupole 2^{nd} order geometric aberrations and the 2^{nd} order dispersion [33] leaving only the higher order terms due to finite sextupole length and partial overlap of the pairs.

Final Focus

The Final Focus is the place where beam size, shape and phase are modified in order to produce collisions. The basic requirements are zero dispersion, zero chromaticity and beams crossing with the same phase at the IP. These requirements result to be more difficult owing to the constraint on ultra low β_y at IP and to the restricted space availability (since detector needs to be installed as close as possible to the IP). Other problems are originated by the presence of detector solenoid, vacuum requirements and alignments. Figures 1.14 and 1.15 show the lattice in the Final Focus for the High Energy Ring and a zoomed view of the Interaction Region. The lattice is derived from the Linear Colliders Final Focus [34, 35, 36, 37] but with important original elements:

- Crab sextupoles inclusion
- Two sextupoles, in phase with IP at beam waist location, upstream chromaticity correction sections, so improving the available demagnification and bandwidth
- All bends are of the same sign
- A different H bending angle before and after the interaction point to compensate for the ± 33 mrad beam crossing angle
- Total bending defined by the polarization constraints at the Spin Rotators (spin precession in dipoles), as described later.

QDo

The requirement of very low beta involves the final quadrupoles to be very close to the Interaction Point. These are very small (6 mm thick) superconducting magnets, named $QD0$ [38], ensuring a gradient of -1.025 T/cm (for HER), enough to focus the High Energy Beam. Chromaticity suppression is achieved using sextupole couples as in the arcs, with a transport matrix between them corresponding to $-I$. Initially the (more sensible) vertical chromaticity is minimized and then the horizontal one. Additional weak sextupoles and octupoles are added to correct second order chromaticity, due to off momentum particles. To compensate for the effects of Detector solenoid, counter acting solenoids are installed together with a tilt compensation applied to the magnets close to the IP. The parameters obtained at the IP are listed in Table 1.3

Chromaticity suppression

Detector compensation

Polarization

To understand the NP properties the beams are required to have the highest possible polarization. Longitudinal polarization is required at

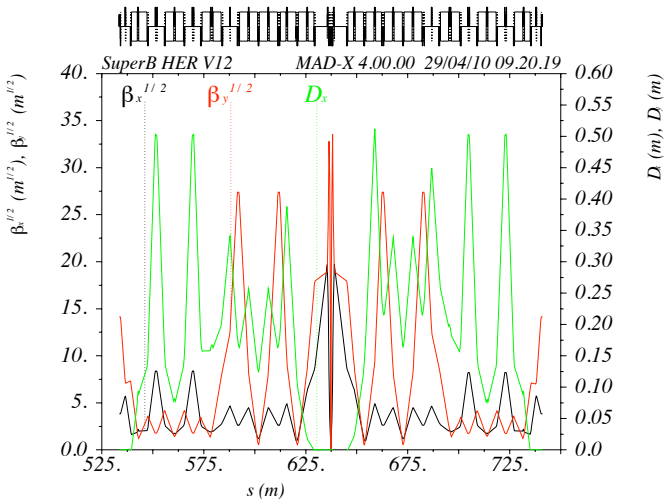

(a) *Lattice functions.*

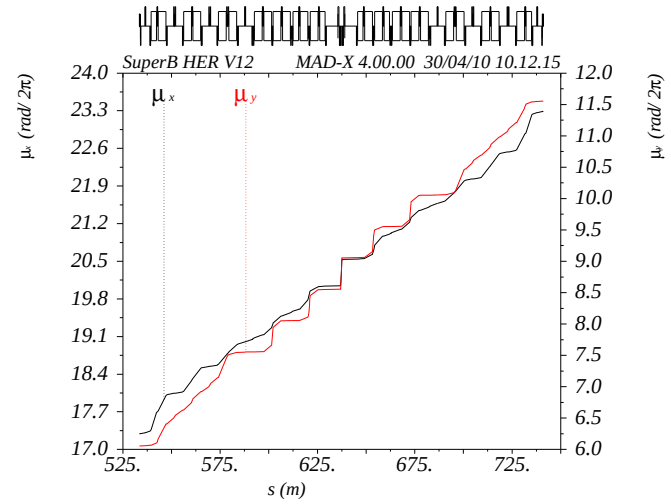

(b) *Phase advance.*

Figure 1.14: SuperB Lattice functions. HER V 12, Final Focus

the IP, while in the arcs, where there are no vertical bends, only a vertically polarized beam travels undisturbed. According to Thomas-BMT equation [39] for spin precession in electromagnetic fields, longitudinally

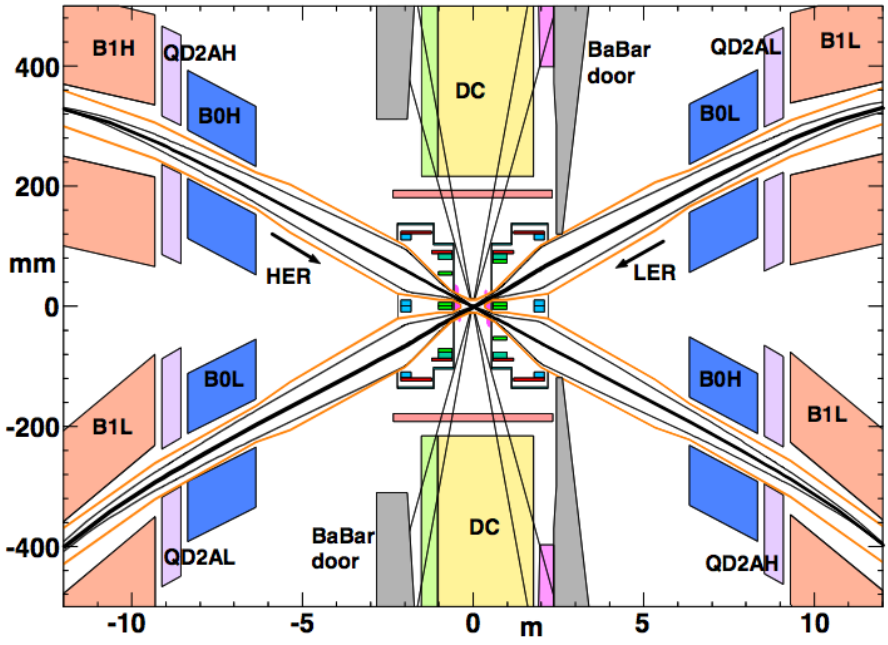

Figure 1.15: Layout of Interaction Region. Note the asymmetric scales for the two axis

	HER (e^+)	LER(e^-)
beam energy (GeV)	6.70	4.18
beam current (A)	1.89	2.45
β_y^* (mm)	0.25	0.21
β_x^* (mm)	26	32
ϵ_y^* (pm)	5.0	5.8
ϵ_x^* (nm)	2.0	2.41
crossing angle (θ)	$\pm$33 mrad	

Table 1.3: Interaction Point parameters with V12 lattice

polarized particles in a vertical field (horizontal bend) have a precession of

$$\psi = (1 + \frac{g-2}{2})\frac{E}{m_e}\theta$$

where ψ is the precession angle, $\frac{g-2}{2}$ is the anomalous magnetic moment for electrons, E the energy of the particles, m_e the electron mass and θ the bending angle of the magnets. This relation imposes a strong constraint on the total bending in the IR. In the actual design, vertically polarized electrons are injected in the LER, and a total rotation of 90° in the transverse plane (x-y) is provided by Spin Rotator solenoids before the interaction region. Than the horizontally polarized spin precess in the dipole magnets between the spin rotator and the IP of 270° in the horizontal (x-s) plane arriving at the IP longitudinally polarized. In the current design SR are placed in the LER since the lower energy allows less drastic changes of the lattice and smaller magnetic fields. The SR are placed between the arcs and the FF and the magnet strengths in the FF are adjusted accordingly to accomplish the needed bending angles that provides the 270° spin precession. Coupling introduced by the solenoids is corrected using a FODO cell, tuned to have transformation matrices in the two planes T_x and T_y

$$T_x = -T_y = \begin{pmatrix} -\cos\psi & -2r\sin\psi \\ \frac{1}{2r}\sin\psi & -\cos\psi \end{pmatrix}$$

where ψ is he total spin rotation given by the solenoids and $r = \frac{pc}{eB}$.

The polarization obtained is of 70% with a life time of 20 minutes.

Long straight section

The long straight section opposite to the IP hosts injection and radio frequency cavities (RF) and it may also be used to change the machine betatron tunes during operation. Beams are injected in the horizontal plane for both rings. The first 3π cell is made longer to accommodate the septum at its center and to insert two kickers on both sides of the cell to realize a closed orbit bump. The lattice function are modified as shown in Figure 1.16 to allow more efficient fast kicks. For both rings the RF cavities are placed as far as possible from the precedent bend, so that sincrotron radiation load is minimized. There are currently 8 RF cavities for LER and 14 for HER.

The beta-functions and dispersion for the complete SuperB HER and LER V12 lattices are shown in Figure 1.17.

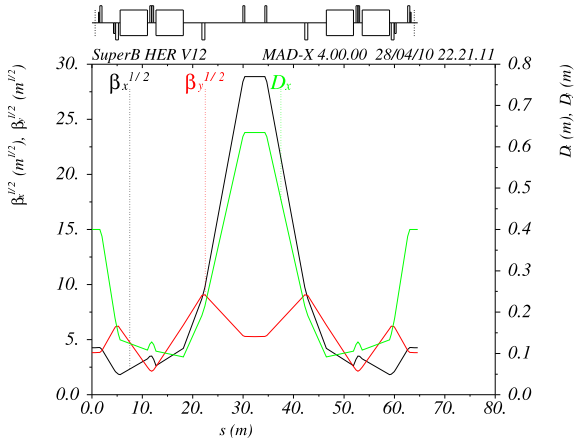

Figure 1.16: SuperB Lattice functions. HER V 12, injection cell

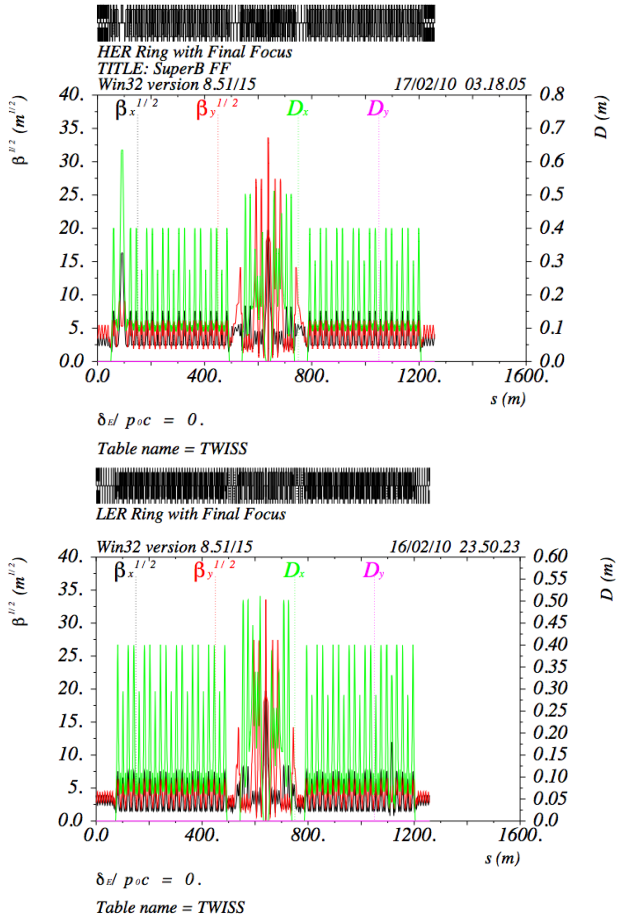

Figure 1.17: SuperB Lattice functions. HER V12 (left) and LER V12 (rigth)

2 LOW EMITTANCE TUNING

Emittance

Luminosity is the key feature for the SuperB project. One of the parameters, that mainly influences the Luminosity, is the machine emittance in the two planes (see eq. 1.5).

The design emittances for SuperB HER (for example) are of 2 nm rad in the horizontal plane and of 5 pm rad in the vertical plane. These values are already inclusive of unavoidable effects increasing the natural emittance of the lattice, like Intra Beam Scattering (IBS), but are requiring a perfect machine lattice. In fact the SuperB "perfect" magnetic lattice produces a vertical emittance of 10^{-38} m rad (dominated only by quantum effects due to synchrotron radiation), and an horizontal equilibrium emittance of 1.26 nm rad. Imperfections in the magnets positioning modify these values considerably introducing orbits distortions and coupling, that readily increase the vertical and horizontal emittances to values even higher then those introduced by IBS. In particular vertical emittance, that is approximately zero in the design project, is strongly influenced by the presence of these errors.

Imperfections in magnets positioning

It is then important to determine the tolerated alignment errors.

The introduction of realistic alignment errors in the lattice produces effects on the orbits that are not negligible and may lead to the loss of the beam even before defining a closed orbit. In the lattice the beam orbit is controlled by diagnostics instrumentation like Beam Position Monitors (BPM) and dipole correctors, respectively to define the orbit and to correct it with small local kicks.

Closed orbit correction

In practice, by means of an accurate choice of the applied corrector strengths it is also possible to choose the orbit which "produces" minimum emittance. This process needs to be simulated and carefully studied before the accelerator construction. For what concerns the best orbit definition,this kind of simulations is also useful to improve machine performance during the running periods.

It is extremely important to provide a set of tolerances for alignment, so that at the construction stage the magnets be positioned with the required accuracy.

All the efforts to obtain the design emittance

The whole of efforts to obtain machine emittance nearly approaching the design values, only knowing the monitor readings and having correction dipole kickers as unique tools, is called Low Emittance Tuning (LET). This procedure includes: a) the simulation of magnet misalign-

ments, b) positioning of BPM's, orbit and coupling correctors in the magnetic lattice, and c) the definition of an algorithm to correct the beam so to achieve the lowest possible emittance.

2.1 MISALIGNMENT ERRORS

The first step of LET procedure is the simulation of the positioning errors in the lattice magnets. For any element in the machine the possible misalignement errors to be considered are:

- horizontal displacement Δx
- vertical displacement Δy
- longitudinal displacement Δs
- tilt around longitudinal axis $\Delta\psi$
- tilt around horizontal axis $\Delta\phi$
- tilt around vertical axis $\Delta\theta$

These degrees of freedom are schematically represented in Figures 2.1.

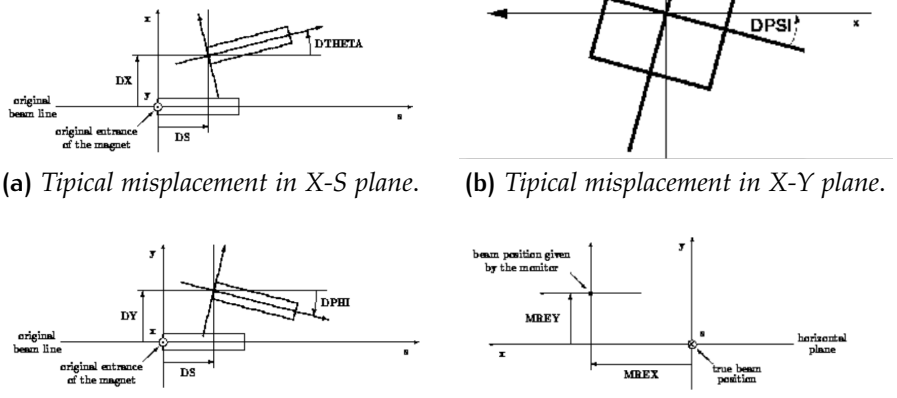

(a) *Tipical misplacement in X-S plane.* **(b)** *Tipical misplacement in X-Y plane.*

(c) *Tipical misplacement in Y-S plane.* **(d)** *Tipical monitor reading errors.*

Figure 2.1: Possible misalignment errors in a ring

Displacements and tilts around the beam axis ($\Delta\psi$) are studied. These errors, when applied in different elements, have different influences on the beam behavior. For example a displacement in the x plane of a quadrupole produces the effect of a kick in the horizontal plane, while the same displacement in a sextupole is equivalent to the introduction of a new quadrupole in the lattice. This may be seen directly from the equations describing the effect of the elements on the orbit. The effect of an "ideal" quadrupole is to provide a kick in both transverse planes given by

$$x' = -kx$$

$$y' = ky$$

where (x, y) are the ideal orbit coordinates, k is the quadrupole strength and $x' = dx/ds$ and $y' = dy/ds$ are the position divergences. In the case of a displacement error $(\Delta x, \Delta y)$ the orbit variations x' and y' may be written as:

Quadrupole misalignment

$$x' = -k(\Delta x + x)$$

and

$$y' = +k(\Delta y + y)$$

which may be solved leading to

$$x' = -k\Delta x - kx$$

and

$$y' = +k\Delta y + ky$$

showing that the effect of the displacement is to have in each plane either the quadrupole focusing effect and a kick proportional to the displacement of the quadrupole. The vertical kick introduced by this imperfection generates vertical dispersion and so vertical emittance growth.

The same may be seen for a sextupole of strength K_s. The orbit variation is described by

$$x' = K_s(x^2 - y^2)$$

$$y' = -2K_s xy$$

where the inclusion of misplacement $(\Delta x, \Delta y)$ leads to

$$x' = K_s(x^2 - y^2) - 2K_s x\Delta x + 2K_s y\Delta y + K_s(\Delta x^2 - \Delta y^2) \quad (2.1)$$

$$y' = -2K_s xy + 2K_s x\Delta y + 2K_s y\Delta x - 2K_s(\Delta x\Delta y) \quad (2.2)$$

Sextupole misalignment

In this case at the sextupole location a fictitious quadrupole of strength $2K_s\Delta x$ and a fictitious skew quadrupole of strength $2K_s\Delta y$ are generated together with small kicks in the two planes.

In general, all misalignments may be described as new elements in the lattice and this allows an easy discussion and understanding of the effects produced on the beam behavior. The influence of kicks affect only orbit and dispersion, while the introduction of horizontal sextupole displacement introduces quadrupole components that modify the β-functions of the lattice. The worst effect on the emittances is the coupling effect due to skew quadrupoles terms deriving from quadrupole tilts ($\Delta\psi$) and vertical sextupole displacements. The coupling introduced in the equations of motion in the two planes "transports" part of the oscillation from the horizontal to the vertical plane (see Appendix), producing a very sharp vertical emittance growth emphasized by the big difference between the emittances.

These errors are not in practice independent so it is necessary to study them when they are present at the same time in the lattice, as it is in reality. In the optic of the construction of a table of tolerances, to evidence the contribution to the final emittance of every kind of error, in the simulations, the effect of the different errors will be studied independently and then the presence of all wished imperfection will be considered in a cumulative simulation. In this way it will be possible to evidence the most influent kind of misalignments and to give less tight tolerances to the least influent ones.

Truncated distribution at 2.5 σ

To simulate these errors in the perfect machine lattice, random values with a truncated gaussian distribution, with a properly selected variance σ, are extracted. The distribution is truncated at 2.5 σ to avoid the effect of tails that are unlikely to exist, and would spoil the simulations. Figure 2.2 shows an example of the effective distribution of misalignments in the horizontal plane applied to the quadrupoles of SuperB arcs lattice.

Worst case misalignment

This distribution of errors is realistic if every element of the lattice is positioned separately. In the case of SuperB this is not the case. Quadrupoles and sextupoles are often on the same support, reducing a lot the relative misalignments between the two magnets. This is also true for the Final Focus Interaction region elements that are placed on the same support, due to the small space availability.

In the following simulations, this kind of correlation is never taken into account. As a consequence two elements, that in practice will be misaligned by 50μm one respect to the other in the simulations might result misaligned by 500μm. Therefore the final tolerances proposed

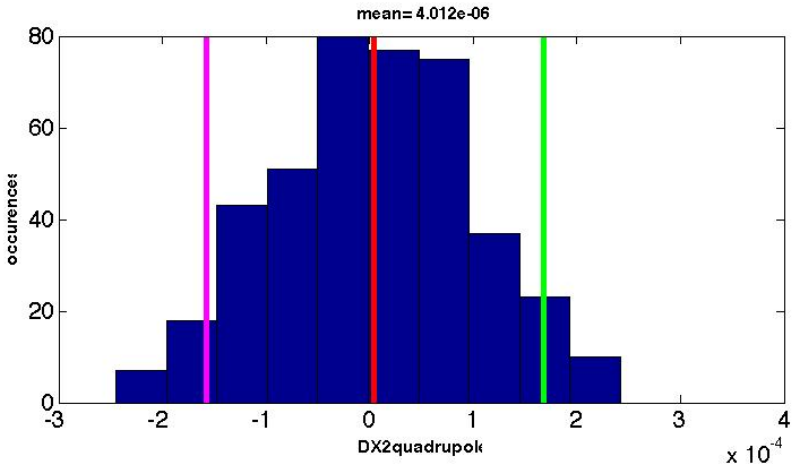

Figure 2.2: Distribution of applied vertical alignment errors on Quadrupoles. Truncated Gaussian at 2.5σ

by the simulations will be more restrictive respect to the really needed ones.

Monitor reading errors

Monitor reading errors

LET is meant to simulate real "beam orbits": for this reason it is necessary to include in the simulations also monitor reading errors that will affect orbits reconstruction, producing a wrong knowledge of the effective machine performance and suggesting a wrong correction to be applied. The errors on the BPM may be of two kinds (Figure 2.1 (d)):

- turn by turn reading error (resolution)
- scale calibration error (electronics)

Turn by turn errors are introduced in the simulations systematically for all the necessary orbit readings, randomly selecting this values form gaussian distributions.

The scale errors may be further subdivided in two classes: offset errors, represented by Δx and Δy for BPMs and amplification errors (multiplicative factors in front of every reading). Only monitor offsets are considered in the simulations that will be presented, while scale amplification errors will be introduced in future simulations.

2.2 CORRECTION PATTERN

Once the machine magnets are misaligned, the closed orbit varies and may be out of control: this affects the beam emittance. Therefore it is necessary to include in the lattice corrector magnets and diagnostics to measure and correct the closed orbit.

The position and number of these elements that would lead to the best correction and orbit sampling is an other parameter which has to be chosen during the LET procedure. The sampling and correction schemes represent difficult choices, even if some key rules may be followed:

- Put monitors at every Quadrupole and Sextupole
- Put correctors in high beta regions

The condition on monitor positions is due to the fact that quadrupole are responsible for orbit focusing, i.e. particles in these elements reach the maxima or the minima of the orbits according to the sign of quadrupole. Therefore quadrupoles are optimal sampling points to determine the path followed by the particles. However, for sake of simplicity in the simulations the monitors are ideally placed nearby the quadrupoles[1].

The requirement for monitors at the sextupoles is determined by the strong effect that their imperfections generate on the orbit and by the relevance that this elements have on the correction. In fact monitors in the sextupoles allow to tune the orbit more precisely to avoid (or take advantage of) the quadruple and skew quadrupole fields generated by their misplacements or by off axes orbit.

Often in the lattice quadrupole and sextupole are in couple and in this cases only one monitor is sufficient.

The second condition has to be verified in order to optimize the influence of the dipole correctors (see Appendix). So, ideally, an Horizontal (Vertical) Corrector should be placed near a Focusing (Defocusing)[2] Quadrupole. At the same time the opposite (Horizontal correctors near Defocusing quadrupoles) has to be true in order to control the orbit divergence. Since a compromise needs to be found and this has to be true for both planes, if the correctors are bidirectional, the central point between two quadrupoles of opposite sign is the best compromise position, if it is available.

1 This is also required by the simulation code that does not allow element superposition.

2 focusing and defocusing are defined in the horizontal plane

Anyway these are indicative recipes, as other elements are present in the lattice and therefore the choice of the position is not a "free parameter".

The simplest procedure to determine the optimal correction pattern is to use, as a starting point, all possible correctors and monitors, filling all available spaces in the lattice. Then the least influent monitors and correctors are removed and the correction procedure is run again to evaluate the new pattern. This iterative procedure can be repeated.

In our simulations a comparison will be made using two different set of correctors and monitors. The correctors installed have no physical length at the moment, but they are inserted in the lattice only if enough space for a true element is available.

2.3 STEERING PROCEDURE

Correction is the third final step of LET. At this stage a technique is developed to calculate the particular set of kicks ensuring the lowest possible emittance. Obviously different corrections lead to different orbits and to different final emittances; the difference among different kick selections will be shown to outline the importance of this passage.

In the present simulation two previously used techniques will be used, together with a new techniques proposed by P.Raimondi. These procedures are known as Orbit Free Steering, Dispersion Free Steering [40], and, the new one, Coupling and β-beating Free Steering. All the techniques relay on the construction of Response Matrices.

2.3.1 Response Matrix technique

Orbit Free Steering

As an example, let us concentrate on the Orbit Response Matrix (ORM) used in Orbit Free Steering . If M monitors and N correctors are available, the ORM is an M×N matrix, where each element represents the change in orbit at the monitors given the change of a single corrector. In matrix formalism, we may write:

$$\vec{R} = \mathbf{ORM} \ \vec{K} \ ; \tag{2.3}$$

where $\vec{R}$ is the BPM readings vector and $\vec{K}$ is the vector of the kicks. In the linear approximation the matrix is determined as $ORM_{i,j} = \frac{\Delta R_i}{\Delta K_j}$, i.e. the measurement change at the i^{th} BPM (i from 1 to M) due to the change of the j^{th} corrector kick of ΔK_j (j form 1 to N).

To calculate the correction it is necessary to invert the relation 2.3, but this is not possible for non-squared matrices. In this case ORM may be decomposed in it's singular value decomposition (SVD) [41], given by: *SVD*

$$svd(ORM) = TSV^t$$

where T and V are respectively an $M \times M$ and a $N \times N$ orthogonal matrices ($T^tT = 1$ and $V^tV = 1$) and S is a diagonal $M \times N$ matrix. The following relations exist, defining Singular Left vectors u (M components) and Singular Right vectors v (N components)[3]:

$$ORM^t u = \sigma v \tag{2.4}$$

$$ORM\, v = \sigma u \tag{2.5}$$

where u are columns of T, v are columns of V and σ are the elements of S. The vectors v and u represent respectively the kick singular vectors and the monitor reading singular vectors: according to equation 2.5, when a kick singular vector v is applied to the accelerator the response is proportional to the corresponding monitor reading singular vector.

There are many possible decompositions, so in general is selected the one for which the elements of S are in decreasing ordered.

The solutions of the equation that describes the perfect orbit given a particular monitor readings vector $\vec{R}$ *Correction kicks evaluation*

$$\vec{R} + \mathbf{ORM}\,\vec{K} = \vec{0} \tag{2.6}$$

may now be determined, obtaining the correction kicks:

$$\vec{K} = -VS^{-1}T^t\vec{R}. \tag{2.7}$$

where S^{-1} is the pseudo inverse of S which is formed by replacing every non zero entry by its reciprocal and transposing the resulting matrix.

Very small eigenvalues σ_i (large i) correspond to singular solutions of the system 2.6, where combinations of correctors (the kick singular vectors associated to that σ) lead essentially to localized small bumps in the measured orbits as shown in Figure 2.3. For this reason, the correction is regularized setting to zero the $\frac{1}{\sigma_i}$ in S^{-1} that correspond to the smaller singular values σ_i. *Singular solutions regularization*

In Figure 2.4 a simulation on SuperB lattice shows how the rms monitor readings after correction and the rms kick strength applied, vary,

3 there are at most min(M,N) singular values, and a corresponding number of singular vectors

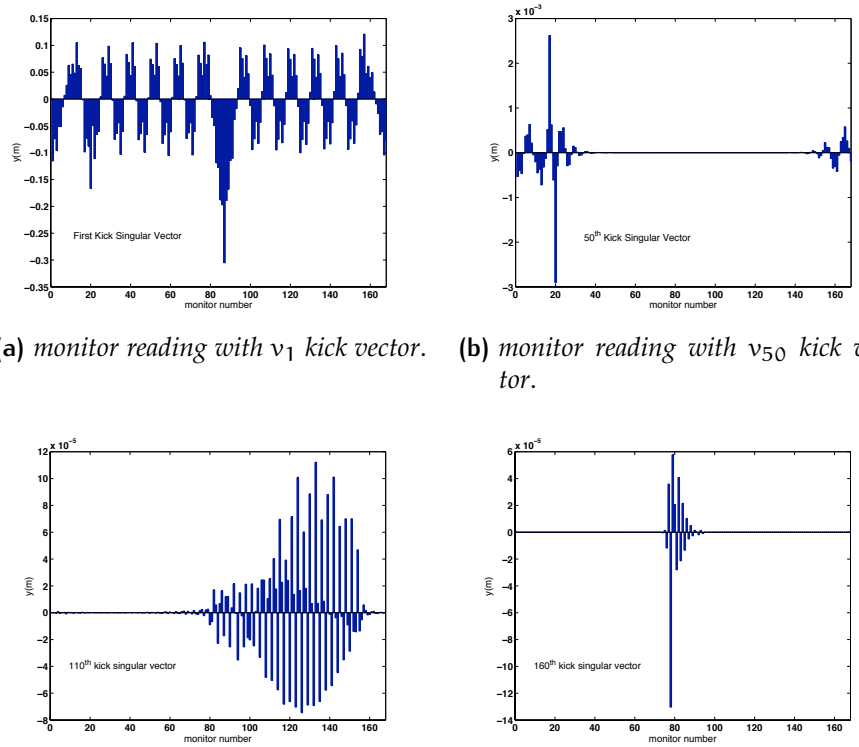

(a) *monitor reading with ν_1 kick vector.*

(b) *monitor reading with ν_{50} kick vector.*

(c) *monitor reading with ν_{110} kick vector.*

(d) *monitor reading with ν_{160} kick vector.*

Figure 2.3: Effect of some Kick singular vectors on the orbit in the vertical plane ($N = M = 168$).

using an increasing number of kick singular vectors in the correction and regularizing to zero the rest of the solutions (for every i in the x axis the kicks vectors form i to N are regularized). The typical elbow pattern is observed, making evident that tuning the correction to use a lower number of kick singular vectors leads to an optimal correction while keeping small rms kicks.

Response matrices are widely used in accelerator Physics. In effect the ORM matrix can be used to perform other studies, like the detection of misbehaving monitors or the calculation of linear optics[42].

The other techniques presented in the following are modifications of the ORM, defined to consider parameters related to non linear effects of elements in the lattice, like sextupoles.

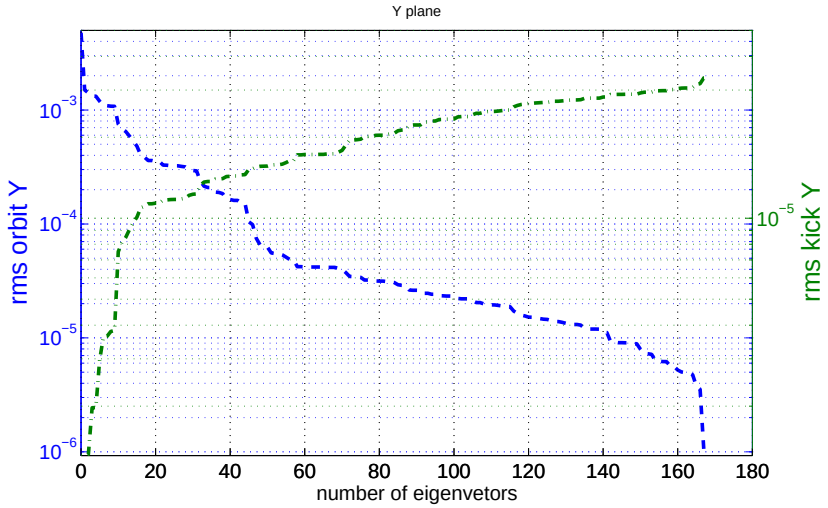

Figure 2.4: rms corrected Y closed orbit (m) and rms Kick applied (rad) vs number of eigenvectors used (ordered by decreasing eigenvalue)

2.3.2 Dispersion Free Steering

Dispersion Free Steering

The calculations of the kicks described above is improved by the introduction of Dispersion Free Steering. This technique applies the same concepts described for Orbit Free Steering to the study of the dispersion. The Dispersion Response Matrix (DRM) is defined as:

$$\vec{\eta} = \mathrm{DRM}\,\vec{K}. \tag{2.8}$$

with $\vec{\eta}$ the dispersion at monitors, calculated as

$$\vec{\eta} = \frac{\vec{R}_{+\frac{\Delta E}{E}} - \vec{R}_{-\frac{\Delta E}{E}}}{2\frac{\Delta E}{E}}$$

where $\vec{R}$ may be the x or y coordinates at monitor and $\frac{\Delta E}{E} = 2.5\,10^{-3}$ is a small energy deviation (since the dispersion is defined as the change in orbit due to a energy deviation).

In order to use a common set of kicks $\vec{K}$ to correct a particular measurement of $\vec{R}$ and $\vec{\eta}$, the system of equations 2.6 may be rewritten as:

$$\begin{pmatrix} (1-\alpha)\cdot\vec{R} \\ \alpha\cdot\vec{\eta} \end{pmatrix} + \begin{pmatrix} (1-\alpha)\cdot \mathrm{ORM} \\ \alpha\cdot \mathrm{DRM} \end{pmatrix} \vec{K} = \vec{0} \tag{2.9}$$

with α the relative weight between the two sets of equations. The calculation of the correction kicks $\vec{K}$ follows the procedure explained

above (see 2.7), via the SVD pseudo inversion of the response matrix extended to include dispersion.

Dispersion is influenced by orbit bumps all over the machine, so the bumps may be corrected if the dispersion that they generate is corrected. Also the dispersion correction by itself is useful, to reproduce the design dispersion value, since (as explained in the first chapter) the minimum emittance lattice is determined by a cell lattice that has minimum dispersion in the dipole.

2.3.3 Coupling and β-beating

The Response matrices introduced above are limited to the correction of effects generated by the dipole kicks introduced by misalignments. The coupling introduced by quadrupoles tilts ($\Delta\psi$) and sextupoles vertical misalignments and the additional quadrupole field introduced by the sextupoles horizontal displacements (or off axis orbit), are only partially correctible with this schemes. Usually new skew quadrupoles are inserted in the lattice to correct coupling and quadrupole strengths are tuned to minimize the β-beating effect due to the additional quadrupole terms. Anyway the Response Matrix may be extended to obtain a better control on these effects with a new technique called Coupling and β-beating Free Steering.

Coupling and β-beating Free Steering

Without additional correctors or skew quadrupoles it is possible to measure two new quantities, $\vec{C}$ and $\vec{\beta}$, related to coupling and β-beating. These quantities are calculated as follows:

$$\vec{C} = \begin{pmatrix} \frac{\vec{x}_{+\Delta V} - \vec{x}_{-\Delta V}}{2\Delta V} \\ \\ \frac{\vec{y}_{+\Delta H} - \vec{y}_{-\Delta H}}{2\Delta H} \end{pmatrix} \tag{2.10}$$

$$\vec{\beta} = \begin{pmatrix} \frac{\vec{x}_{+\Delta H} - \vec{x}_{-\Delta H}}{2\Delta H} \\ \\ \frac{\vec{y}_{+\Delta V} - \vec{y}_{-\Delta V}}{2\Delta V} \end{pmatrix} \tag{2.11}$$

where ΔH and ΔV are two fixed kicks applied in the horizontal or in the vertical plane while $\vec{x}$ and $\vec{y}$ are column vectors corresponding to the orbit coordinate at the BPMs. For example the notation $\vec{x}_{-\Delta H}$ represents $\vec{x}$ in presence of a fixed kick in the Horizontal plane of value $-\Delta H$.

Two new response matrices, CRM and βRM are built to satisfy the relations:

$$\vec{C} = \mathrm{CRM}\,\vec{K}_y \tag{2.12}$$

$$\vec{\beta} = \beta\mathrm{RM}\,\vec{K}_x. \tag{2.13}$$

where $\vec{K}_{x,y}$ are kicks vectors in the two planes. Every entry of this matrices is obtained using two correctors at the same time: the one that provides the kick necessary for the calculation of 2.10 and 2.11, that is the same for all elements of the matrix, and the one used to determine that particular response matrix column.

The set of correctors strengths $\vec{K}$ is now requested to constrain also this new quantities, leading to a further modification of equation 2.9:

$$\begin{pmatrix} (1-\alpha-\omega)\,\vec{R}_x \\ \alpha\,\vec{\eta}_x \\ \omega\,\vec{\beta} \end{pmatrix} + \begin{pmatrix} (1-\alpha-\omega)\,\mathrm{ORM}_x \\ \alpha\,\mathrm{DRM}_x \\ \omega\,\beta\mathrm{RM} \end{pmatrix} \vec{K}_x = \vec{0} \tag{2.14}$$

$$\begin{pmatrix} (1-\alpha-\omega)\,\vec{R}_y \\ \alpha\,\vec{\eta}_y \\ \omega\,\vec{C} \end{pmatrix} + \begin{pmatrix} (1-\alpha-\omega)\,\mathrm{ORM}_y \\ \alpha\,\mathrm{DRM}_y \\ \omega\,\mathrm{CRM} \end{pmatrix} \vec{K}_y = \vec{0} \tag{2.15}$$

where ω determines the influence of the new equations on the correction like the parameter α for Dispersion Free Steering[4] and the subscripts x, and y refer to the matrices and vectors restricted in the horizontal or vertical plane.

To avoid that at some BPMs $\vec{C}$ and $\vec{\beta}$ are zero, due to the sinusoidal oscillation introduced by the fixed correctors (see Appendix A.1), a further correction is introduced, where the fixed kicks ΔH and ΔV are applied by correctors with a phase advance of approximately 90° with respect to those used to calculate $\vec{C}$ and $\vec{\beta}$. The complete set of equations is now:

$$\begin{pmatrix} (1-\alpha-\omega)\,\vec{R}_x \\ \alpha\,\vec{\eta}_x \\ \omega\,\vec{\beta} \\ \omega\,\vec{\beta}_{\pi/2} \end{pmatrix} + \begin{pmatrix} (1-\alpha-\omega)\,\mathrm{ORM}_x \\ \alpha\,\mathrm{DRM}_x \\ \omega\,\beta\mathrm{RM} \\ \omega\,\beta\mathrm{RM}_{\pi/2} \end{pmatrix} \vec{K}_x = \vec{0} \tag{2.16}$$

$$\begin{pmatrix} (1-\alpha-\omega)\,\vec{R}_y \\ \alpha\,\vec{\eta}_y \\ \omega\,\vec{C} \\ \omega\,\vec{C}_{\pi/2} \end{pmatrix} + \begin{pmatrix} (1-\alpha-\omega)\,\mathrm{ORM}_y \\ \alpha\,\mathrm{DRM}_y \\ \omega\,\mathrm{CRM} \\ \omega\,\mathrm{CRM}_{\pi/2} \end{pmatrix} \vec{K}_y = \vec{0} \tag{2.17}$$

4 $\alpha + \omega \leqslant 1$

where $\pi/2$ indicates the use of the different correctors.

Equations 2.16 and 2.17 ensure the selection of the orbit that minimizes dispersion, coupling and β-beating, leading to the minimum vertical emittance. This is obtained taking advantage of the passage of the beam off axis in the sextupoles, that generates in the vertical plane a skew quadrupole field and in the horizontal plane a quadrupole field (se eq. 2.1 and 2.2).

The minimum vertical emittance orbit

The effect of the correction is shown evidently in Figure 2.5 where the set of tolerated misalignments (i.e. Table 4.3) is applied and corrected with weights $\omega = 0.01$ and $\alpha = 0.49$, using 65 eigenvectors and 114 correctors. The optimization of this values is described later.

In the plots are shown the beta functions for SuperB HER lattice without Final Focus, after misalignments are applied and after correction. The oscillations induced by the misalignments are clearly mitigated after correcting with the new system of equations, resulting in an effective improvement of the final emittance.

Reiteration of steering

To apply the wright correction Response Matrices need to be measured or simulated. In the case of simulated measurement with SuperB lattice each Response Matrix requires ~ 45 minutes (with 150 correctors) to be fixed. For this reason the matrices used for the calculation of correction are not the perfect ones that would describe the machine in the current state, but often are previously calculated matrices. On the other hand, in practice, matrices do not change much: so even if imperfections may change in time, the same matrices can be used. For these reasons, to improve the results of the correction it is wise to re-iterate the correction. In this case the kicks $\vec{K}_{n+1}$ applied at $n+1$ iteration will be:

Re-iterate correction

$$\vec{K}_{n+1} = svd\,(M)^{-1}\left(\vec{R} + M\vec{K}_n\right) \tag{2.18}$$

where $\vec{K}_n$ are the previous kicks, $\vec{R}$ is the readings vector and M the Response Matrix used. This way to proceed is very useful since it may be possible to calculate all the matrices from the ideal lattice and use them to correct orbits generated in a real accelerator, only using the BPM experimental responses.

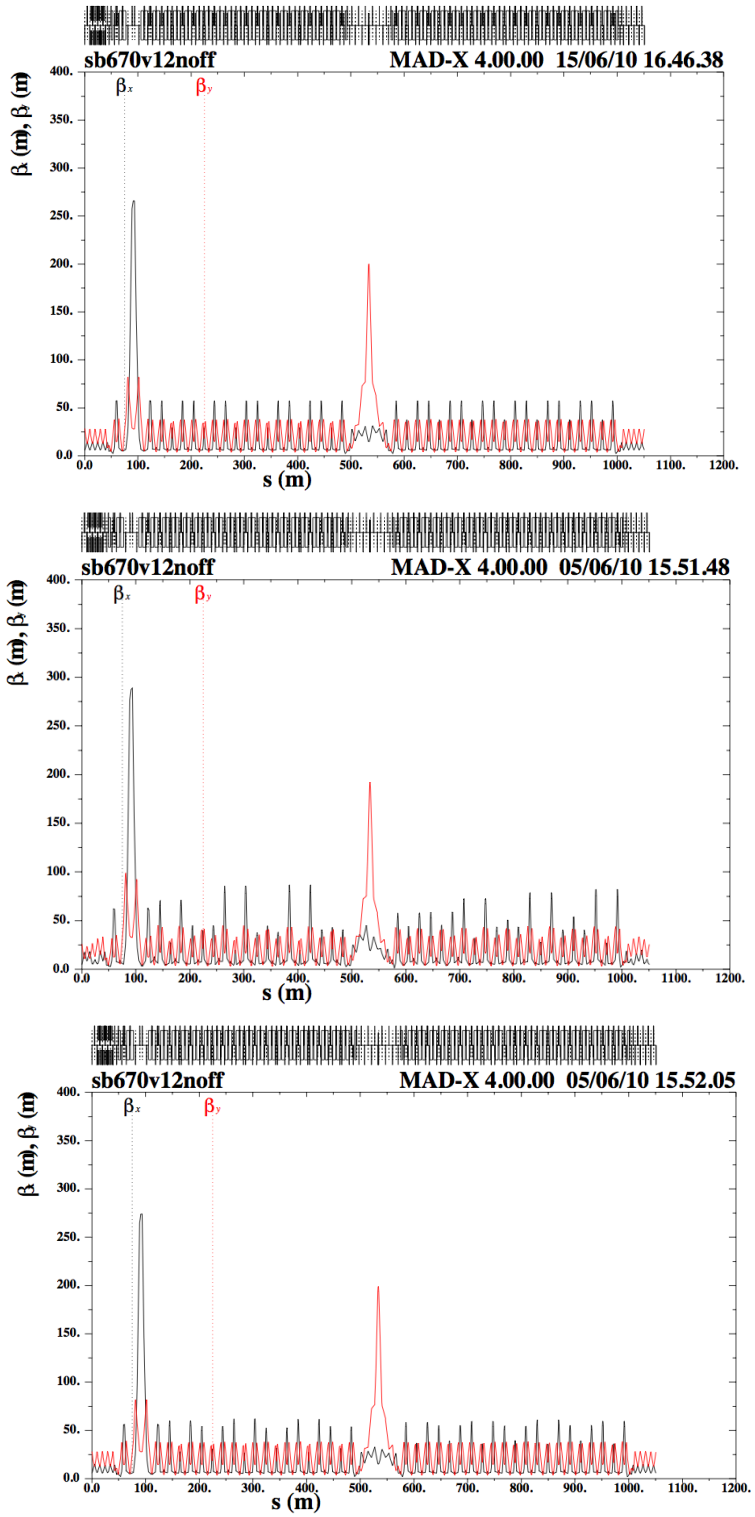

Figure 2.5: Beta functions in SuperB HER lattice without final focus, with 114 correctors and monitors in both planes. Without misalignments (top), with misalignments before correction (center) and after correction (bottom).

2.3.4 Comparison of Correction Schemes

To show how the correction works in more detail, Figures from 2.6 to 2.9 show the effect of the different corrections on rms closed orbit, vertical dispersion, vertical pseudo coupling (effect of horizontal kick on vertical orbit, calculated as in CRM response matrices), and horizontal β-beating calculated as $\frac{\beta_x - \beta_{xDesign}}{\beta_{xDesign}}$.

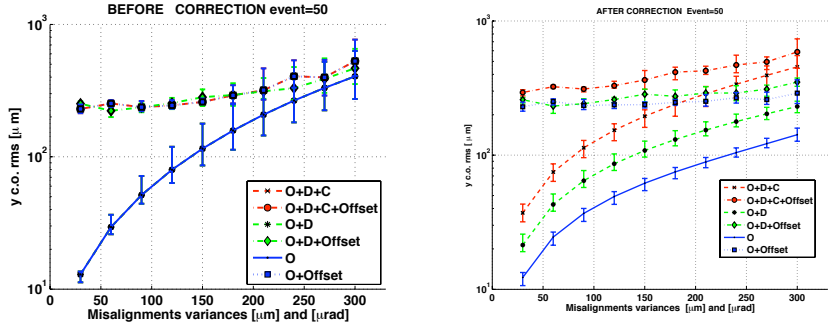

Figure 2.6: Comparison of corrections: Closed Orbit rms

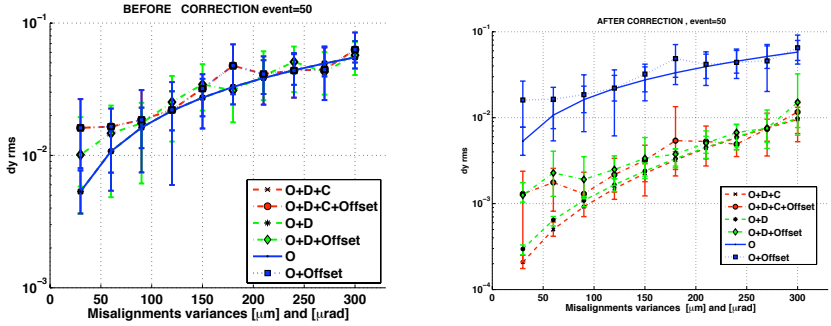

Figure 2.7: Comparison of corrections: Vertical Dispersion rms

Correction comparison

In the Figures the applied error variances range from 0 to 300μm for quadrupoles and sextupoles (on both planes) and from 0 to 300μrad for quadrupole tilts. All the plots on the left side are before correction and those on the right side are after correction. The blue lines show the correction using only orbit steering (O), the green ones considering only dispersion and orbit free steering (O+D) , and the red ones include all the correction schemes (O+D+C). All corresponding simulations have the same seed for the random misalignment of magnets, and so the

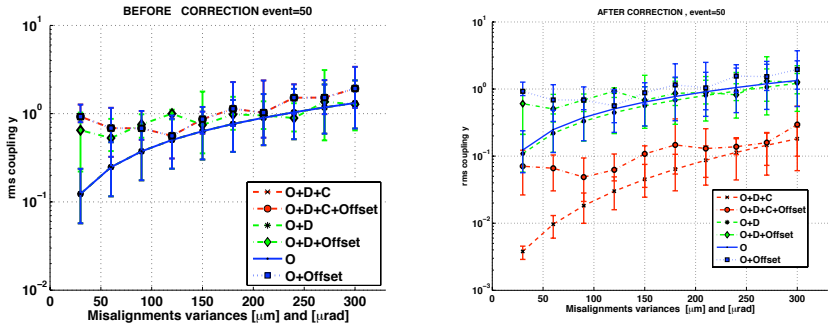

Figure 2.8: Comparison of corrections: influence on horizontal kick on vertical orbit rms

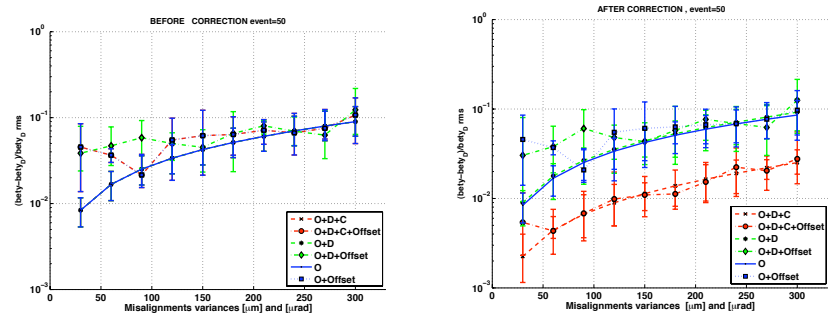

Figure 2.9: Comparison of corrections: $\frac{\beta_y - \beta_{yDesign}}{\beta_{yDesign}}$ rms

same magnet misalignments. In this way the correction comparison is made on exactly the same orbit with the three different schemes. All the corrections relay on the basic relation $\vec{R} + ORM\,\vec{K} = \vec{0}$ where ORM is modified at need and the vector $\vec{R}$ represents the responses of the monitors. This response may be influenced by the misalignment applied ($\vec{R}_L$) or by the errors present on the monitors ($\vec{R}_M$). So the relation may be rewritten as

$$(\vec{R}_L + \vec{R}_M) + ORM\,\vec{K} = \vec{0} \tag{2.19}$$

To investigate also the influence of $\vec{R}_M$ the effect of BPM offset with a variance of 300μm fixed for every simulation but with changing seed, is shown in the Figures (Legend+Offset).

In the Figures from 2.6 to 2.9 it is evident that the use of the correction including all the response matrices leads to a deprecation of the orbit rms of a factor ~ 4, but at the same time improves rms dispersion, coupling and β-beating of a factor 10 to 100.

These observations are not influenced by the presence of monitor offsets. In fact orbit is never less then the magnitude of these errors, but since dispersion coupling and β-beating are calculated by difference of two measurements, correction is not influenced by the presence of these errors.

The lowest vertical emittance

Finally the simulated emittances are plotted in Figure 2.10. The use off all the corrections generally ensures the lowest vertical emittance and therefore this is the best correction scheme to be used in presence of misalignments.

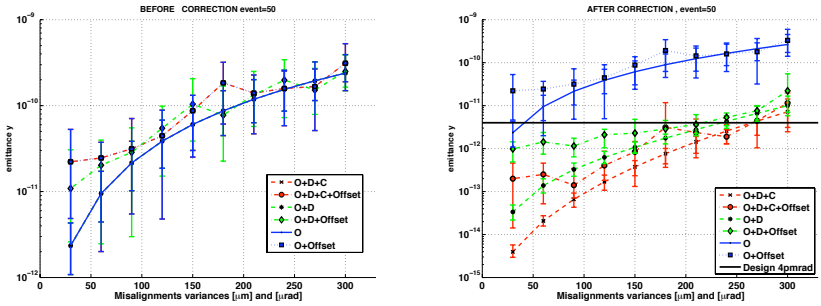

Figure 2.10: Comparison of corrections: ϵ_y

The price to pay is the need to measure six response matrices. Five of these matrices require a double time for calculation, since they are obtained by difference of two orbits. So a factor ~ 10 in time for the measurement of the matrices is required compared to the time needed for pure orbit steering. This problem may be solved by the calculation of matrices from design. The time is still long but it does not need the use of the accelerator. The matrices for the design machine are produced and then may be used reiterating the correction.

As described in this chapter, in LET procedures a great amount of variables enter into play to determine the best emittance in front of a set of misalignments. For this reason all the passages explained above have been included in a single graphical interface, that enables an easy approach to the LET procedures together with a good flexibility in the simulations to be made. The capability of the interface are explained in detail in the next chapter.

3 L.E.T. TOOL

To implement the LET procedure Mad-X[43] and MATLAB[44] are used. Mad-X may be used alone to apply LET, implementing misalignments, installing the new elements, applying correction and doing iterations. Anyway MAD-X does not allow complete freedom. The are three main limitations given by the use of this code:

- **No flexibility in changing the correctors and monitor scheme** This operation requires to install the elements either one by one or by means of macros, but both methods require to act on the lattice structure by hand, while it would be wise to have a procedure able to realize the same kind of positioning even if the lattice itself is modified. This is very important in project design phase, when frequent modifications are applied.

- **Fixed Correction** Correction may not be handled to include DRM, CRM and βRM. As described in the previous chapter, the correction scheme used is very sensible and it is important to be able to tune it appropriately to have a optimal selection of kick values.

- **Limited plots** Plots are limited to few internal variables reducing drastically the graphical capabilities, and the ability to show different variables for the same simulation without producing every time the plots for all variables.

Anyway the use of Mad-X is necessary for the simulations of the accelerator. All the parameters of interest, like emittance, dispersion, closed orbit, ecc. are still calculated within this code.

To solve the problems raised by the use of Mad-X and allow further improvements like the capability to calculate the Response Matrices, a Matlab Graphical User Interface (GUI) was developed (a screenshot of the tool is shown in figure 3.1).

This interface is capable to realize:

- **Interactivity with Mad-X, graphic interface and Mad-X input definition** This solves the first problem. It is possible to define or modify the correctors and monitor distribution in the accelerator in a very quick way. The elements are installed in the lattice

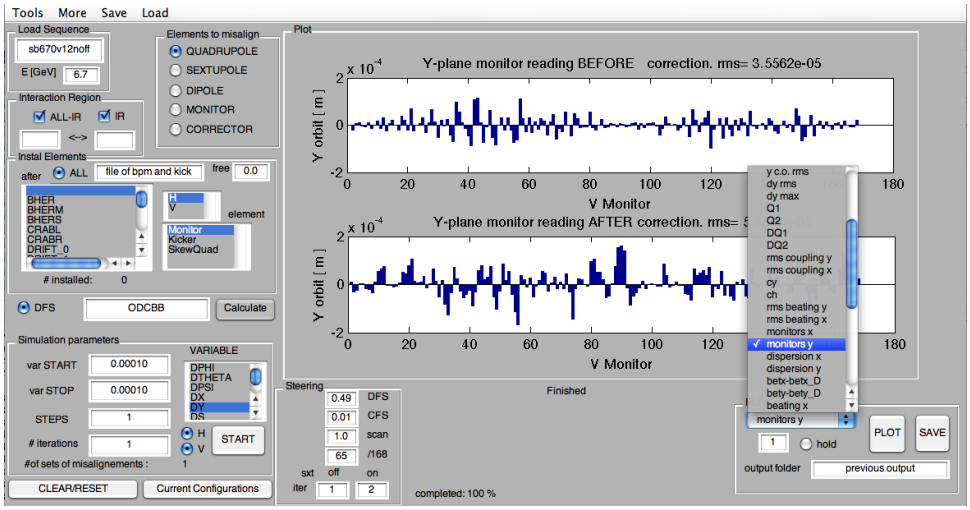

Figure 3.1: Matlab tool built and used for simualtions

sequence using a Mad-X macro written on the simulation input file by Matlab.

- **Dispersion coupling and β-beating Free Steering** Matlab supports all the calculations relative to the correction and feeds the results to Mad-X. Also the response matrix calculation may be triggered from the interface, so that Matlab writes on the Mad-X input all the commands necessary for the measurement of the orbits and then reads the output files to build the matrices, that are saved and may be reloaded in next simulations.

- **Show and save plots** All the variables of interest are stored in files produced by Mad-X. Matlab displays this information in the most appropriate way, according to the kind of simulation wanted (single or multiple errors) and may also give informations about the correction procedure, like kick values at every simulations. The plots of interest may then be saved and edited offline. This may be done at any time since the program saves all the simulations in folders with all the necessary files, and allows, for example, to superimpose simulation results for easier comparisons.

- **Analyze ANY sequence** This is a major advantage of the interface. The tool may quickly analyze any ring, i.e. it is not exclusively dedicated to SuperB.

- **Multiple errors in any element** Also the description of errors requires to modify the code in Mad-X considerably. Using the GUI the errors may be defined simultaneously for any element with the desired distribution variance, so that, for example, quadrupole and sextupole alignment errors may have different distributions in the same simulation.

- **Varying variances** To determine the tolerated values it is interesting to analyze the behavior of the lattice when the variance of the simulated errors changes. This may be done using Matlab in an easier way compared to the use of nested macros and loops in Mad-X, that is actually limited to no more than two level of nesting.

- **Interaction Region Errors** Since the Interaction Region needs special care, it may be wished to assign different misalignment errors to this region, or to study the effects produced in the Final Focus by errors in the arcs. This is again possible using the GUI to define the Mad-X input for this purpose.

Deep mixture of Mad-X and MATLAB

This tool is actually a deep mixture of Mad-X and MATLAB but Mad-X is responsible for all the simulations. The schematic description of the procedure followed by the tool is described in Appendix.

3.1 TESTS OF MISALIGNMENTS

A few tests of the application of the misalignments via the Interface described in the previous section were performed to be confident in the use of the tool. Two situations of misalignment with predictable results were considered:

- With no vertical misalignments, no vertical orbit is expected. In Figure 3.2 the Mad-X output for orbit and dispersion for a machine with random misalignments with 100 μm rms in the x plane for Sextupole and Quadrupoles is shown. As expected, there is no Y orbit nor Y dispersion.

- If only tilts in quadrupoles exist, the orbits will not be affected, while in the Y plane dispersion will appear.

  Figure 3.3 shows orbit and dispersion when 300 μrad rms tilt are applied to quadrupoles. The simulation appears to work properly.

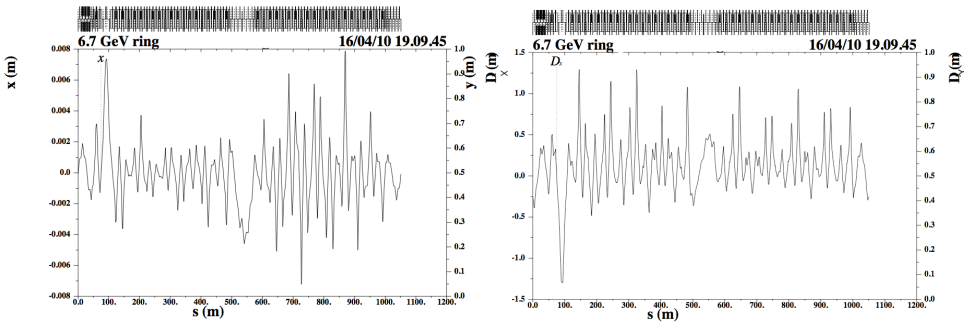

(a) *Orbit* . **(b)** *Dispersion*.

Figure 3.2: Mad-X output for 100 μm X rms misalignment for Quadrupoles and Sextupoles. No correction applied

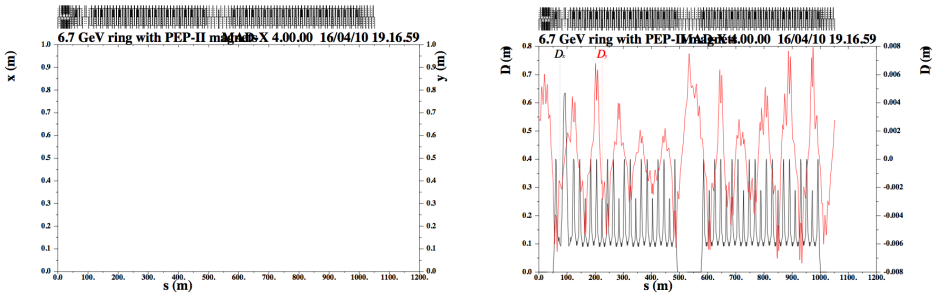

(a) *Orbit* . **(b)** *Dispersion*.

Figure 3.3: Mad-X output for 300 μrad rms tilt for Quadrupoles. No correction applied

To further check that the misalignments are applied correctly the introduction of theoretical predictions, in presence of particular kinds of imperfections, can be useful. The quantities introduced are: the *Orbit Amplification Factor* due to quadrupole vertical displacements and the relations between vertical emittance and sextupole vertical misalignments and quadrupole tilts [45][46].

Amplification Factor

- In presence of quadrupole misalignments (y_{quad}) the root mean square amplitude of the errors and that of the orbit (y_{co}) are related by the amplification factor A as:

$$\sqrt{\langle y_{co}^2 \rangle} = A \sqrt{\left\langle y_{quad}^2 \right\rangle} \tag{3.1}$$

$$A^2 \approx \frac{\langle \beta_y \rangle}{8 \sin^2(\pi \nu_y)} \sum_{quads} \beta_y (K_1 L)^2 \tag{3.2}$$

where ν_y is the vertical tune, the angle brackets represent the average around the machine and $K_1 L$ is the integrated strength of the quadrupoles. The Closed Orbit amplitude is highly influenced by the particular set of misalignments used, so the error distribution is wide and the amplification factor of equation 3.2 represents the average over a large number of machines.
In Figure 3.4 a linear fit is applied to the distribution of rms orbit obtained by 10 simulations for 10 different misalignment variances, showing how, for small errors, the simulations agree.

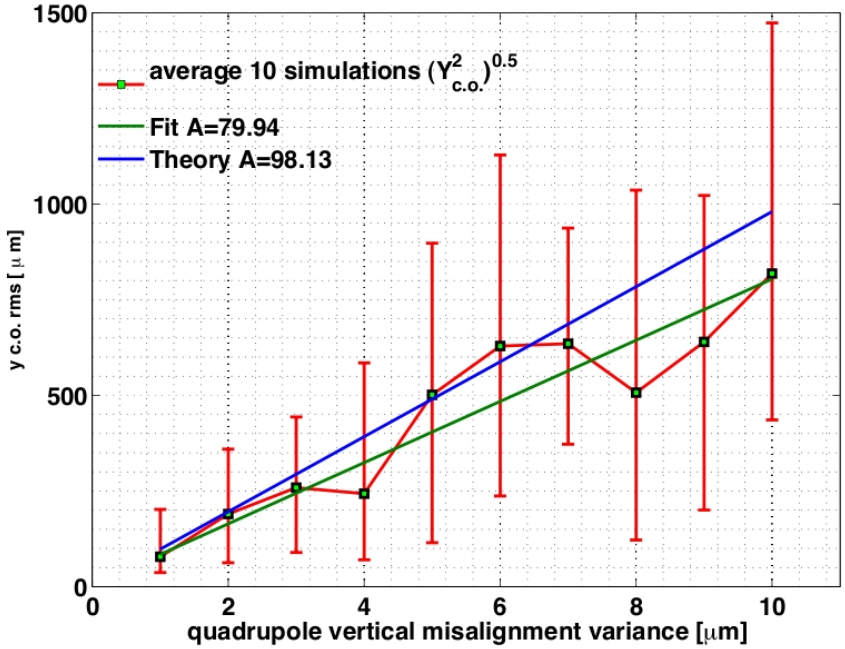

Figure 3.4: Amplification Factor: Closed orbit amplification due to quadrupole vertical displacements

- The second theoretical prediction involves sextupole misalignments. These errors, as discussed in the second chapter, introduce in the lattice the equivalent of a quadrupole in the horizontal plane, a skew quadrupole in the vertical plane and two kicks. This affects the orbit in both planes of the machine, introducing coupling and

β-beating. The vertical emittance is linked to the rms vertical displacement of the sextupoles by the following relation

$$\epsilon_y \approx \left\langle y_{sext}^2 \right\rangle \frac{J_x\,[1-\cos 2\pi\nu_x \cos 2\pi\nu_y]}{4J_y\,[\cos 2\pi\nu_x - \cos 2\pi\nu_y]^2}\,\epsilon_x \sum_{sexts} \beta_y \beta_x (K_2 L)^2 + \left\langle y_{sext}^2 \right\rangle \frac{J_z \sigma_\delta^2}{4\sin^2 \pi\nu_y} \sum_{sexts} \beta_y \eta_x^2 (K_2 L)^2 \tag{3.3}$$

where J are the partition numbers, ν the tunes, β the beta functions, ϵ the emittances and K_2L the integrated strength of the sextupoles. In the second term σ_δ is the rms energy spread and η_x is the horizontal dispersion. Also this equation considers averaging over many machine sets of errors, and again the distribution of emittances will be wide. Figures 3.5 shows these distributions obtained simulating 10 different set of misalignments for 10 different error variances. A quadratic fit of the simulations and the curve described by equation 3.3 are superimposed for comparison to the simulations.

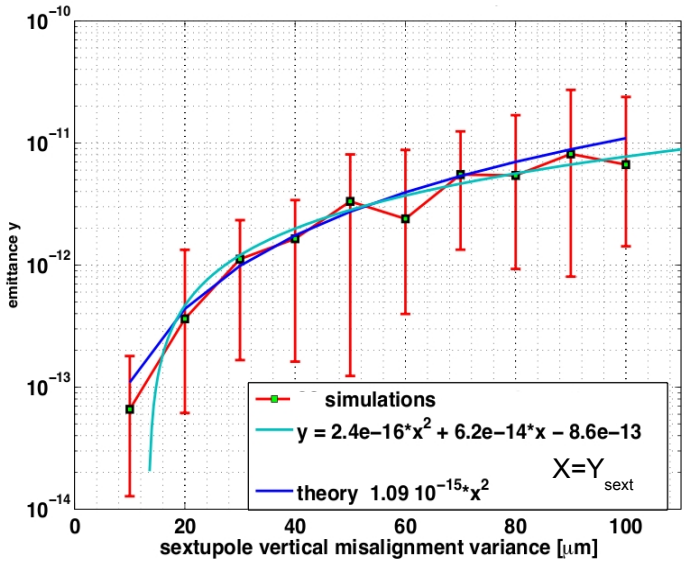

Figure 3.5: Influence of Vertical sextupole displacements on vertical emittance (m rad)

- Also quadrupole tilts in the transverse plane (Δψ), may be analyzed in the same way, and theory again gives an estimate of the

effect of these errors on vertical emittance. The relation between vertical emittance and quadrupole tilts θ_{quads} is:

$$\epsilon_y \approx \left\langle \theta^2_{quads} \right\rangle \frac{J_x\,[1-\cos 2\pi\nu_x \cos 2\pi\nu_y]}{4J_y\,[\cos 2\pi\nu_x - \cos 2\pi\nu_y]^2}\epsilon_x \sum_{quads} \beta_y\beta_x(K_1L)^2 + \left\langle \theta^2_{quads} \right\rangle \frac{J_z\sigma_\delta^2}{4\sin^2\pi\nu_y} \sum_{quads} \beta_y\eta_x^2(K_1L)^2 \tag{3.4}$$

that is exactly the same as the previous one, except for the presence of integrated kick strengths over all quadrupoles. The comparison of 3.4 with simulations (quadratic fit) is shown in Figure 3.6.

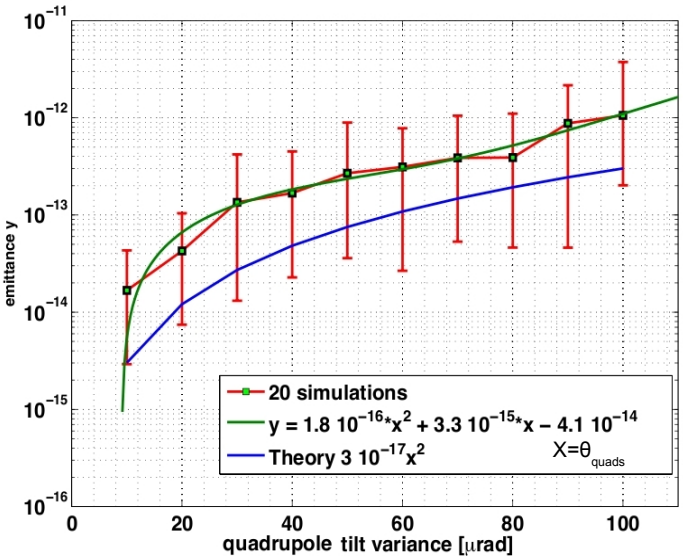

Figure 3.6: Influence of Quadrupole Tilts on vertical emittance (m rad)

The second terms of equations 3.3 and 3.4 are due to the influence of horizontal dispersion on emittance. The quadratic fit is in fair agreement with theory.

This analysis confirms that simulations are consistent with theory.

4 TOLERANCES

With the LET procedure it is possible to determine the emittance obtained in an accelerator with realistic conditions of misalignments. While up to now the final parameters, (and specifically emittance), ere studied for different initial misalignments, the aim of this chapter is to determine the set of misalignments that may be tolerated by an accelerator without exceeding the design values of emittance. This study is pivotal in the design of the machine, since it allows to determine at which level of precision the elements need to be placed in order to obtain the designed Luminosity. In the analysis performed all the errors are considered simultaneously, producing a realistic simulation of the corresponding effects, as the correlations among the different imperfections are also taken into account.

4.1 ANALYSIS SETTINGS

Elements

All the analysis has been performed for the SuperB lattice but the FF section. The Final Focus is not currently considered due to complications given by strong quadrupoles and high beta-functions. For this reason a more sophisticate tuning procedure has to be developed even if the same tools may be used.

The lattice β function (black β_x and red β_y) and the dispersion (green) under study are shown in Figure 4.1.

Through the GUI, 168 monitors and correctors are installed in both planes: they are placed at every quadrupole, sextupole and octupole, if the constraint of a free space of at least 40 cm is fulfilled. At the center of this available space the corrector is placed.

The resulting distribution is abundant for the arcs where there are about 6 correctors per cell. For this reason studies on the optimal minimization of the correctors layout are useful. An example of the result obtained with a restricted set of four correctors and monitors per cell is shown at the end of this chapter.

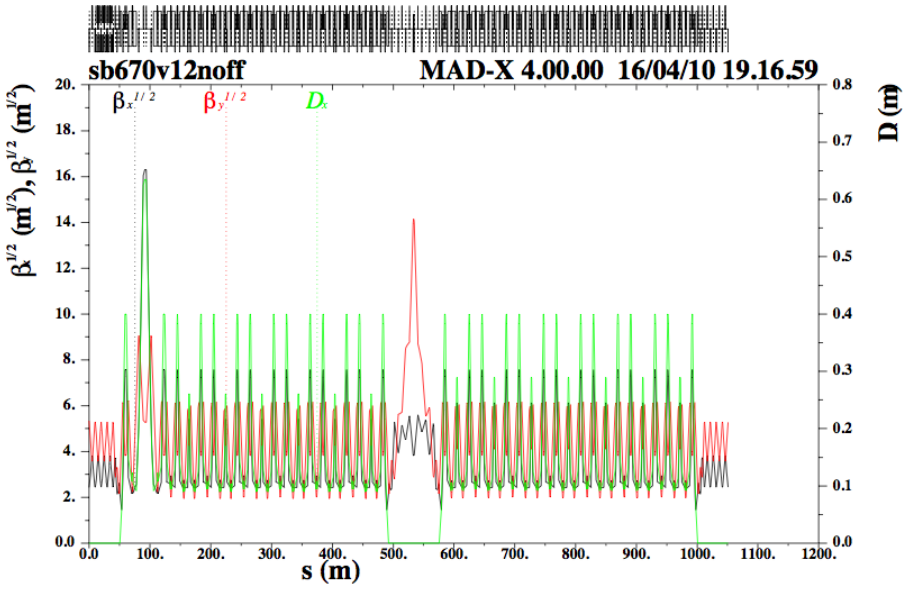

Figure 4.1: Lattice for SuperB (Version V12) without final focus

Correction

To apply the correction we need to measure the matrices for orbit steering, and to set the optimal parameters for correction. Figure 4.2 shows the orbit, dispersion, coupling and β-beating response matrices used for the calculation of the correction kicks.

Two independent kicks are applied to calculate the response matrix in the two directions. The kicks used are: in the X plane 10 μrad, in the Y plane 5μrad. This is chosen because the β_y is generally larger than β_x especially in the region where the fixed kicks (see section 2.3.3) used for calculation of the coupling and β-beating response matrix are selected (long straight in the lattice). With this choice the amplitude of the oscillation induced by the fixed correctors (see appendix A.1) is approximately the same for the two directions. There is no effect on the calculation of the Orbit and Dispersion Matrices given by the selection of this particular kick values.

To use the matrices for the correction in the form described in 2.16, it is necessary to determine the best values of three parameters: the "relative" weights α and ω and the number of kick singular values to be used (kick eigenvectors). To determine the optimal values of the weights α and ω Table 4.1 reports the vertical emittance ϵ_y for various couples of relative weights .

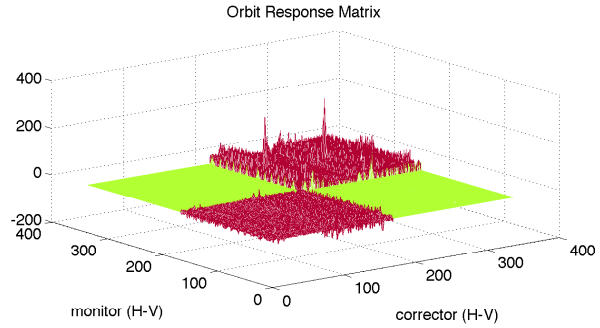

(a) *Orbit Response Matrix.*

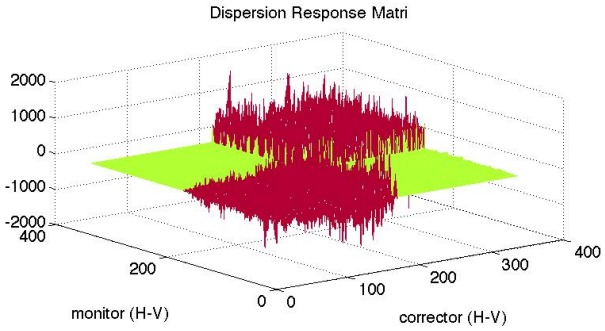

(b) *Dispersion Response Matrix.*

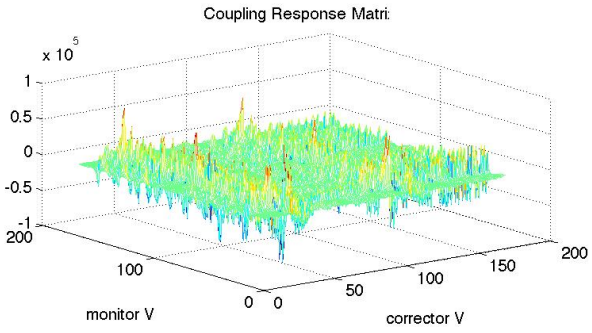

(c) *Coupling Response Matrix (y plane).*

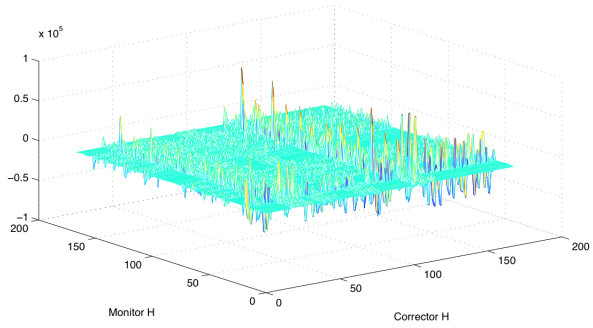

(d) *β-beating response matrix (x plane).*

Figure 4.2: Response Matrices

	DFS (α)							
CFS (ω)	0%	10%	20%	30%	40%	50%	60%	70%
0% (0)	9.641	2.324	0.152	0.461	0.847	1.129	1.293	1.354
0.5%(0.00125)	3.307	**0.0484**	**0.0307**	**0.024**	**0.021**	**0.021**	**0.023**	**0.025**
1% (0.0025)	3.612	**0.052**	**0.039**	**0.033**	**0.028**	**0.025**	**0.022**	**0.021**
4% (0.01)	1.481	0.061	**0.043**	**0.043**	**0.042**	**0.041**	**0.039**	**0.038**
8% (0.02)	5.284	0.155	**0.054**	**0.047**	**0.044**	**0.043**	**0.042**	**0.043**
12% (0.03)	7.375	0.401	0.067	**0.052**	**0.046**	**0.044**	**0.044**	**0.044**
40% (0.1)	3.377	1.238	0.732	0.537	0.394	0.117	0.082	**0.065**
80% (0.2)	16.113	1.683	1.116	0.824	0.710	0.628	0.547	0.482

Table 4.1: ϵ_y pm rad **vertical emittance** for various relative weights. Every entry is result of one simulation with 100 µm vertical misalignment in the vertical plane corrected only in the vertical plane. Bold entries for $\epsilon_y < 6 \times 10^{-2}$ pm rad. CFS is Coupling and β-beating Free Steering and DFS is Dispersion Free Steering

Every entry is result of one simulation with 100 µm vertical misalignment in the vertical plane for quadrupoles and sextupoles, corrected only in the vertical plane with 65 eigenvectors. The same seed is used for all simulations. The "relative" weight omega is a misleading quantity since it's influence is 4 times bigger than that of the parameter α since it appears in front of four matrices instead of only one. As a consequence in the Table 4.1 is reported an effective percentage of influence on the correction.

To help in the selection of the weights the entries that are below 6×10^{-2} pm rad are evidenced in bold. The very broad minimum area allows to select among these values with freedom. In this sense the values chosen in this region are optimal for all simulations performed also with different variances of error distributions. It is also evident from the Table that using the two methods alone (first row and first column) does not lead to optimal results. The selected values for the simulations are $\alpha = 0.49$ and $\omega = 0.01$, being at the center of the vertical emittance minimum area.

Figure 4.3 shows vertical emittance (decreasing, left log scale) and rms vertical kicks strength (increasing, right linear scale), for the three

different orbit steering techniques, as a function of the number of kick singular vectors used in the SVD inversion of the Response Matrices (see section 2.3.1). This vectors are ordered for decreasing eigenvalues and it is expected that the last kick singular vectors are small and localized bumps and do not influence the correction, while in fact they increase the root mean square kick. For this reason they may be excluded form the calculations.

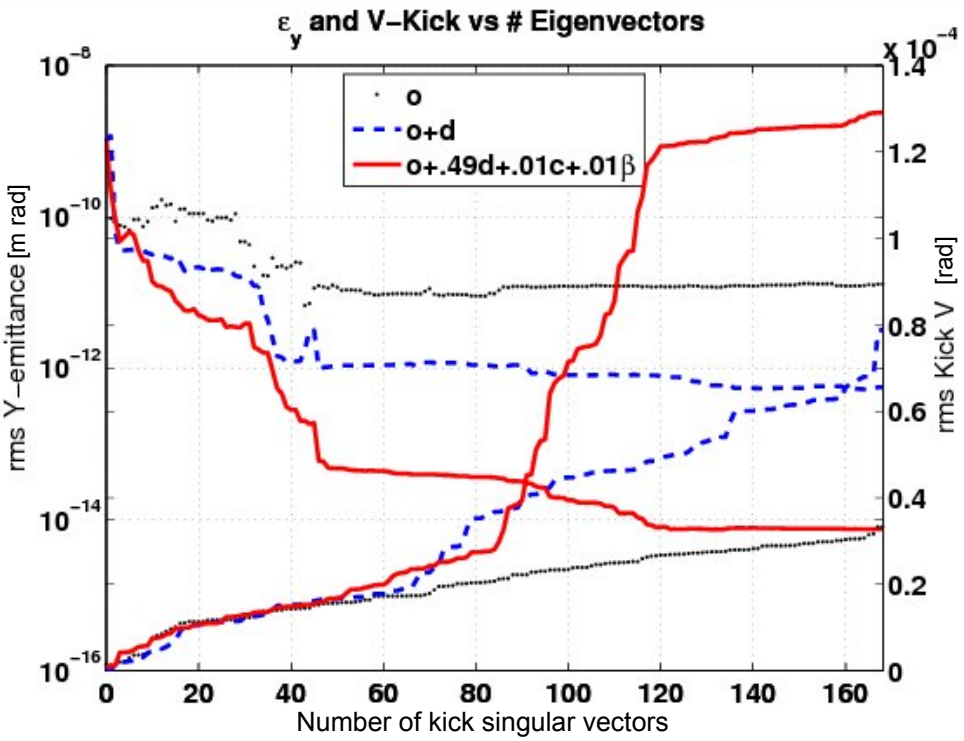

Figure 4.3: Vertical emittance and applied kick rms as a function of the number of kick singular values used. The dotted black lines are built using only orbit correction (o), the segmented ones using Orbit and Dispersion Free Steering (o+d, $\alpha = 0.5$), and the red lines add to the blue ones Coupling and β-beating Free Steering (o+d+c+β, $\alpha = 0.5$, $\omega = 0.01$)

The correction applied in the simulations uses 65 kick singular vectors out of 168.

In Figure 4.3 the improvement given by the use of CRM and βRM Response Matrices is again evident, producing for any set of kicks applied, vertical emittances a factor 10 better than Dispersion Free Steering and a factor 100 better then Orbit Free Steering.

4.1.1 Correction reiteration

Having set all the parameters for a single correction, the optimal scheme for correction reiteration must be determined.

In the previous chapter it has been shown that all response matrices are calculated when errors are still not applied to the lattice to allow a speedier computation. This choice has two advantages: firstly it allows to proceed in the calculation only once and not for every different set of errors; secondly it allows to be sure that the calculation will terminate. The disadvantage is that the response matrices obtained are not perfect for the misaligned lattice. To solve this problem correction reiteration is applied following equation 2.18.

In the SuperB cell lattice without misalignments, the nonlinear effect due to sextupoles should cancel. To limit the effect of "imperfect" sextupoles on the orbit a pre-correction is performed with sextupoles off. Pre-correction steering may also be reiterated. In Table 4.2 is shown the obtained vertical emittance varying the number of iterations with sextupoles on and off, for vertical misalignment of quadrupole and sextupole with 100 μm variance.

Pre-correction

iterations			
sxt off	sxt on	ϵ_y (pmrad)	time (s)
1	1	6.526 10^{-2}	23.6
1	**2**	**2.371** 10^{-2}	**37.8**
1	3	3.290 10^{-2}	48.4
1	4	4.094 10^{-2}	60.1
2	1	3.655 10^{-2}	35.8
2	2	3.876 10^{-2}	47.2
2	3	4.501 10^{-2}	59.8
2	4	1.584 10^{-2}	73.8

Table 4.2: Vertical emittance obtained with different correction reiterations

The choice of the number of iteration is also driven by time issues. Good correction and time consumption are obtained for 1 iteration of pre-correction and 2 iterations of complete correction.

4.2 TOLERANCE TABLE

To study the machine tolerated errors, the analysis considers all the tolerated errors at the same time and not one by one. Furthermore there is no comparison with the machine model in the correction scheme, so no fitting procedures are to be used, but only data from simulations or experimental measurement, if available. The errors that will be considered are: quadrupole tilts ($\Delta\psi$), quadrupole and sextupole misalignments (Δx and Δy) and monitor offsets.

The aim of the computation is to define the values of the rms misalignments that, will produce, after correction, vertical emittances of less than 5 pm rad and horizontal emittances of less than 2 nm rad.

Many procedures may be used to define these tolerated errors. Evidently the different misalignments are strictly correlated both by the coupling (introduced in the orbit by imperfections like tilts and vertical displacements of sextupoles) and by the alignment systems that may be used. For this reason it is important to study the error kinds separately and then merge the results in a single simulation to evidence the influence of the single errors and determine the maximum tolerated values for every one of them. The following procedure is used:

1. misalignments of sextupoles, misalignments of quadrupoles, tilts of quadrupoles and BPM offsets are analyzed separately for increasing variance form 100 to 500 μm or μrad (5 simulations for 6 different variances). The emittance obtained after correction for these errors are shown in Figure 4.4.

2. a smaller interval of variances is selected, for all the different errors, close to the region that leads to emittances distribution completely contained under 0.1 pm rad.

3. these interval of variances are applied together and the tolerated values are selected as the maximum ones giving a distribution completely contained under the 0.5 pm rad threshold.

As a result of this analysis the combination of all the imperfections gives a vertical emittance of less than 1pm for the tolerated values.

Figure 4.4 shows that with the use of the new correction scheme that considers also coupling and β-beating (see 2.3.3), errors like monitor offsets and quadrupole displacements have small effect on the final emittance and the tolerated values may be higher.

On the other hand the big influence of sextupoles misalignments was expected either owing to the particular lattice composition of SuperB

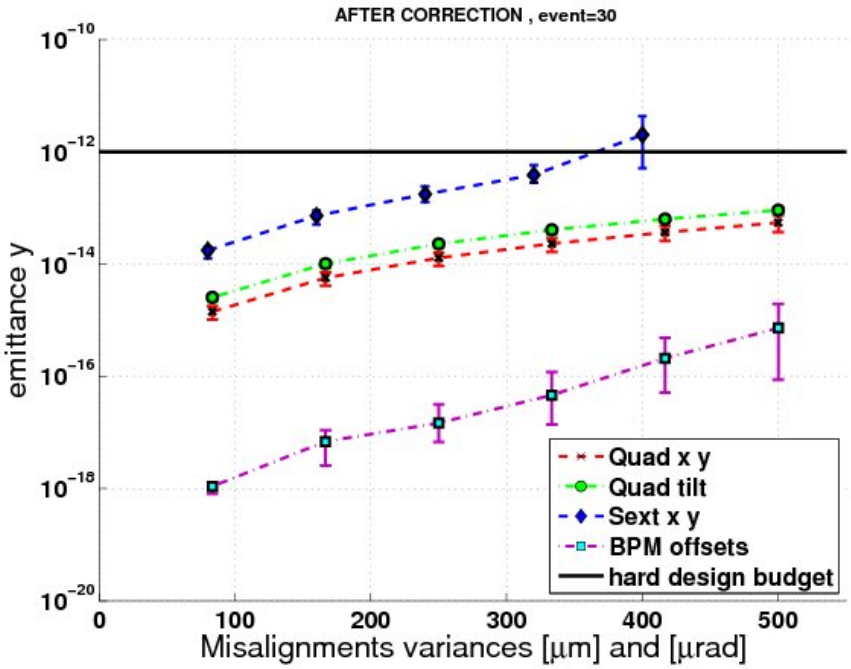

Figure 4.4: Vertical Emittance (m rad) vs: misalignments of sextupoles, misalignments of quadrupoles, quadrupole tilts and BPM offset errors. Every point is the average of 5 simulations.

either to the fact that sextupoles are used with this correction scheme as correctors themselves so that their positioning becomes more relevant.

The tolerated values resulting from the procedure above are listed in Table 4.3.

rms BPM misalignment	400 μm
rms quadrupole vertical misalignment	300 μm
rms quadrupole tilt	300 μrad
rms sextupole vertical misalignment	150 μm
rms sextupole horizontal misalignment	150 μm
BPM horizontal resolution	1 μm
BPM vertical resolution	1 μm

Table 4.3: Tolerance table for $\epsilon_y < 1 \times 10^{-12}$ m rad **vertical emittance**

The emittances obtained applying at the same time all the values of Table 4.3 (but the BPM resolutions) are shown in Figure 4.5, before and after correction. All the simulations presented lead to values of the verti-

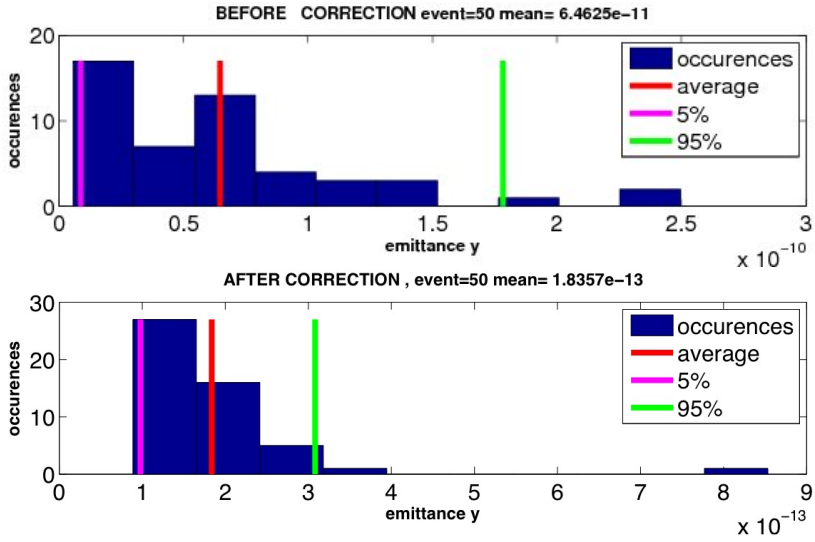

Figure 4.5: Vertical emittance (m rad) in presence of misalignments tilt and BPM offset errors from Table 4.3. 50 simulations

cal emittance lower than 1 pm rad, and on the average 0.184 pm rad are obtained. For the same simulations, the average horizontal emittance is 1.27 nm rad and the distribution is contained under 1.35 nm rad. For the determined tolerated values both the emittances distributions are much lower than the thresholds determined by IBS (5 pm rad for the vertical emittance and 2 nm rad for the horizontal emittance) while the errors applied are well within the achievable technology limits.

4.2.1 Monitor Reading Errors

Monitor resolution errors influence the orbits to be corrected and for this reason they need special care and understanding.

To evidence the effect produced by the BPM resolution these errors have been studied in the perfect lattice (so that, looking back at 2.19, only $\vec{R}_M$ is present). Their influence on the vertical emittance before and after correction is shown in Figure 4.6.

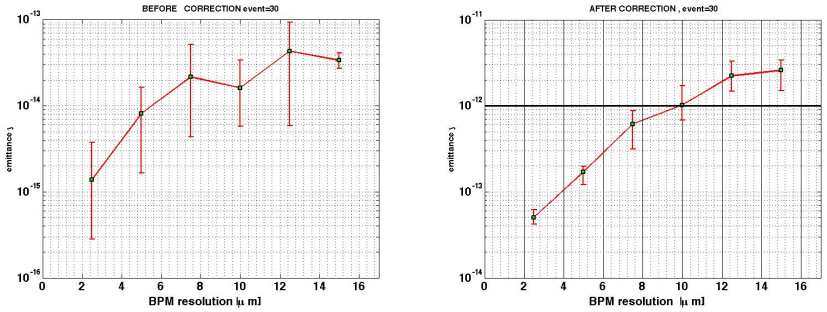

Figure 4.6: Vertical emittance (m rad) due only to increasing BPM reading error before and after correction

Before correction the emittance increases due to the application of kicks to the perfect orbit in the pre-correction: the orbit readings are non zero, due to the BPM errors, so the kicks applied are effectively only spoiling the orbit. After correction there is no improvement, since the quantities used for correction have random values. While monitor offsets are fixed throughout all the simulation and in the case of dispersion coupling and β-beating (defined by a difference of orbits) their effect systematically cancels, for monitor reading errors the influence is unpredictable and changes at every orbit reading. This sensitive influence on the other hand may became useful since it allows to detect misbehaving BPMs using the Response Matrices (see for example [47]).

Including a 1 μm BPM reading error, the simulations of the imperfections in Table 4.3 returns a wider distribution but still gives values not much grater than those obtained using perfect monitors (Figure 4.7).

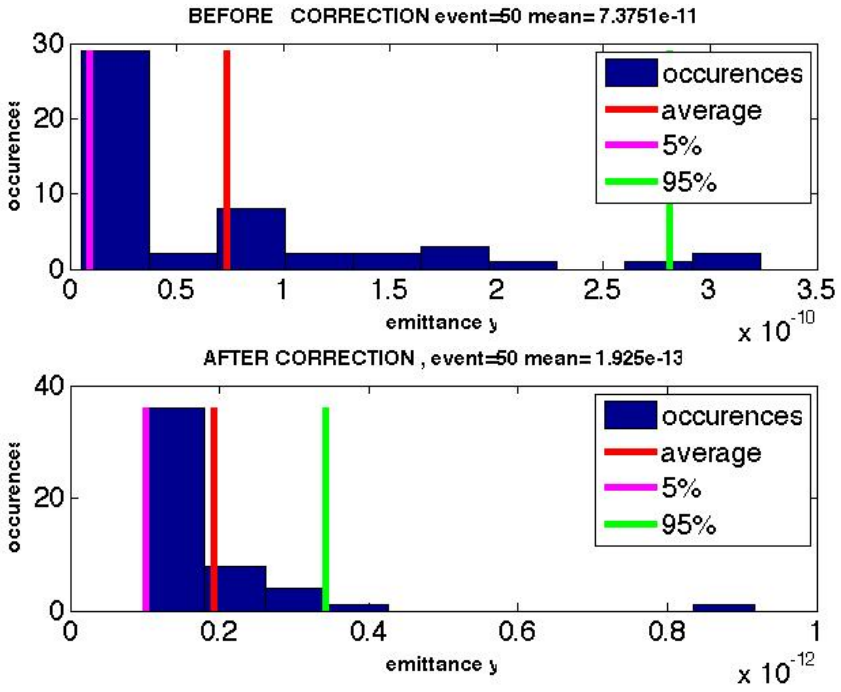

Figure 4.7: Vertical emittance (m rad) in presence of misalignments, tilts, BPM offset errors and BPM resolution from Table 4.3. 50 simulations.

4.3 SMALLER SET OF CORRECTORS

To show the relevance of the distribution of BPM and corrector magnets, the same procedure is applied removing particular correctors and monitors from the previous disposition. The set of installed elements now counts 114 horizontal and vertical correctors and monitors (instead of 168), placed as in the complete simulation. The analysis is performed using the same correction parameters and misalignment variances (Table 4.3). The number of kick singular vectors used is changed to 50 to optimize kick rms and final vertical emittance. The vertical emittance obtained before and after correction for 50 simulations is summarized in Figure 4.8.

The average final vertical emittance, with this smaller set of correctors, is 2 times larger than the one obtained with the complete set and the distribution overruns the 1 pm threshold for a 5%. The reduced number of correctors and monitor is an advantage for cost and operation, but on the other hand, diagnostics and handles on the machine behavior are never in surplus in an accelerator. A trade off has to be found.

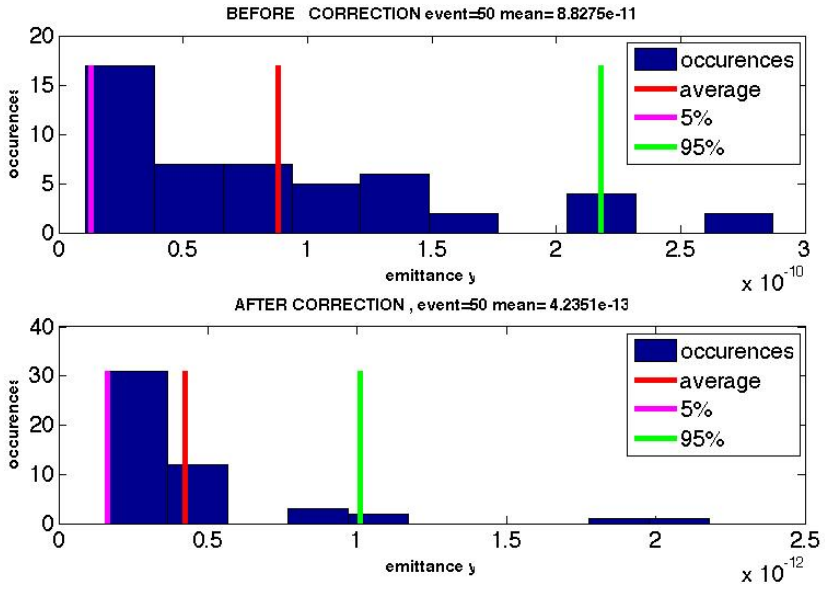

Figure 4.8: Vertical emittance (m rad) in presence of misalignments, tilts, BPM offset errors and BPM resolution from Table 4.3, with a smaller set of 114 correctors and monitors instead of 168. 50 simulations.

On the other hand by this simulation it is clear that the number of correctors and monitor may be reduced without affecting the correction.

5 CONCLUSIONS

"I have made the wrong mistakes"

Thelonious Monk
(after an unsatisfactory Jazz improvisation)

Misalignments, tilts and resolution of BPM influence the performance of SuperB collider, affecting the final vertical emittance and drastically reducing the machine achievable luminosity. For this reason it is critical to determine how well magnets have to be placed and which kind of correction should be applied to achieve results as close as possible to the design.

In this thesis the analysis of alignment imperfections has been performed considering everything that may influence the final emittance: the position of the diagnostic and correctors and the calculation of the correction.

This procedure, called L.E.T., has been carried on by means of a new tool with a graphical interface, ensuring the analysis to be developed in an easy, fast and flexible way. The tool relies on Matlab and Mad-X, (used respectively for interface and simulation) and may either set all the parameters of the simulations and calculate all the necessary quantities automatically, including the Matrices necessary for the correction. The same tool is also an interface to the simulations result, so allowing to have access to many relevant variables (for example the final vertical emittances).

All the simulations are performed considering only information retrieved from monitors and the correction of the orbit generated by random misalignments is performed using only dipole correctors (no coupling correctors). The values of the correction kicks are obtained via Singular Value Decomposition (SVD) of a composition of Response Matrices for orbit (ORM), dispersion (DRM), coupling (CRM) and β-beating (βRM). Three different possible correction schemes are analyzed, and it is shown that the introduction of Coupling and β-beating Free steering is fundamental for the final results, enabling the correction to minimize the emittance.

Coupling and β-Beating

The correction calculation is tuned for best performance and applied systematically to determine the maximum tolerated misalignments for SuperB HER arcs quadrupoles and sextupoles and the needed BPM resolution.

An interval of tolerated values is determined independently for every misalignment studied, setting a low threshold respect to the total target. This intervals are then further optimized (to obtain a single value for every imperfections) in a simulation where all the imperfections are studied at the same time. This allows to have tolerated values that consider correlations between the imperfections and that lead to simulations always under the design value.

Applying random distributions of errors with the determined tolerated values of misalignments to the design lattice a vertical emittance (after correction) of 0.183 pm rad is achieved, much lower than the design of 5 pm rad. This incites for further simulation of further errors, like the introduction of the Final Focus magnets and the study of field errors. Also the effect of BPM reading errors, that influence the correction calculation, are investigated showing that currently available monitors may be used in SuperB design without influencing the tolerated values of misalignment. The tolerances reported are for the SuperB HER but the same procedures are being applied to LER: in the present Study Final Focus is not included.

$\epsilon_y < 5\ pm\ rad$

To evidence that optimization is possible a different scheme of correction with a smaller number of monitors and correctors was also simulated and compared to the "complete" one. After removing one third of the installed correctors and monitors the average vertical emittance is double with respect to the complete set, but still one order of magnitude under the design limit.

The tolerances obtained in this thesis are necessary to determine the achievable Luminosity in realistic conditions of machine imperfections, to determine the optimal corrector and monitor distribution and to define an adequate correction method. The new correction method requires to be tested on a true beam, and the DIAMOND light source has accepted to give machine time in this purpose. In fact the results obtained are focused on SuperB Arcs but the procedure and tool developed may be rapidly and easily used by any accelerator.

A THEORY BACKGROUNDS

"Whatever is not expressly forbidden is mandatory."

R.P Feynman

A.1 ACCELERATOR THEORY

Some definitions that may be useful for a reader that does not have any background on accelerator physics are listed here. For a complete resume of Accelerator Theory and formulae see [48] and [26].

Local Reference System

The local reference system used in circular accelerators is shown in figure A.1

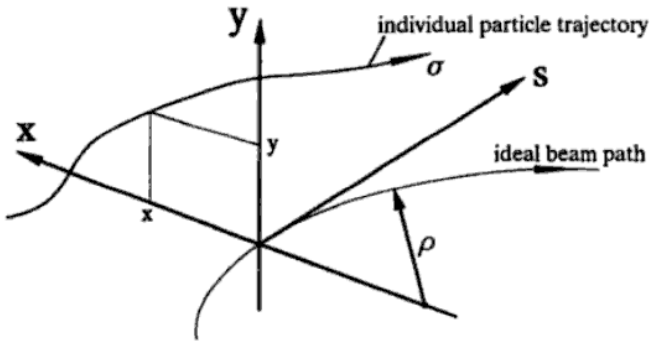

Figure A.1: Local Reference System

The reference orbit consists of a series of straight line segments and circular arcs. It is defined under the assumption that all elements are perfectly aligned. The accompanying tripod of the reference orbit spans a local curvilinear right handed coordinate system (x,y,s).

The local s-axis is the tangent to the reference orbit. The two other axes are perpendicular to the reference orbit and are labelled x (in the bend plane) and y (perpendicular to the bend plane)

Twiss parameters.

Twiss parameters describe the motion of particle of an acelerator in terms of the ellipse occupied in the phase space (x,x'). This parameters are β, α and γ function.

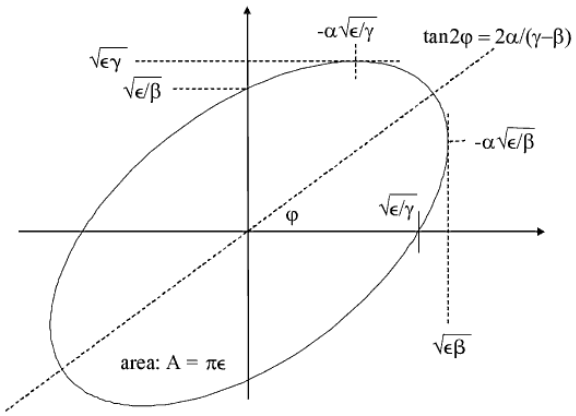

Figure A.2: Twiss parameters

The β function describes the amplitude of the oscillations in the accelerator at every location.

Emittance

Emittance ϵ is the area of the ellipse in phase space occupied by the particle of the beam. A small emittance represents a beam that occupies little space and has very small transverse momentum. In the case of electron beams this quantity is determined by the equilibrium between the synchrotron radiation damping and the quantum fluctuations[26].

Dispersion

The displaced equilibrium orbit for momentum $p = p_0 + \Delta p$ is given in terms of the momentum dispersion function D,

$$x(s) = D(s)\frac{\Delta p}{p_0}$$

with $D(p, s + C) = D(p, s)$ (C is the Circumference and s the position on it.). D satisfies an inhomogeneous Hill's Equation

$$D'' + (K_x\frac{p_0}{p} - \frac{1}{\rho^2}\frac{\Delta p}{p_0})D = \frac{1}{\rho}\frac{p_0}{p}$$

where ρ is the radius of curvature for p_0, and K_x represents the strength of the quadrupoles in the ring.

Coupling

The equation of motions in the transverse planes are:

$$x'' + K_x(s)x = S(s)y + R(s)y' + \frac{1}{2}R(s)'y$$

$$y'' + K_y(s)y = S(s)x + R(s)y' + \frac{1}{2}R(s)'y$$

with

$$S = \frac{B'_{skew}}{B\rho} \quad R = \frac{B_s}{B\rho}$$

$$B' = \frac{\partial B}{\partial x} \quad B'_{skew} = \frac{\partial B_{skew}}{\partial x} \quad R' = \frac{\partial R}{\partial s}$$

The S and R terms arise from skew quadrupole and solenoidal fields. The equations are linear periodic coupled equations, and show the influence of one orbit on the other.

Tune

The number of oscillations per turn in a cyclic accelerator is the *tune*,

$$\nu = \frac{1}{2\pi}\oint\frac{ds}{\beta}$$

Tune may not have any value in an accelerator. To avoid resonances (see [26]), for which the influence of magnetic elements would determine beam loss after some turns, this quantity needs to be an irrational number.

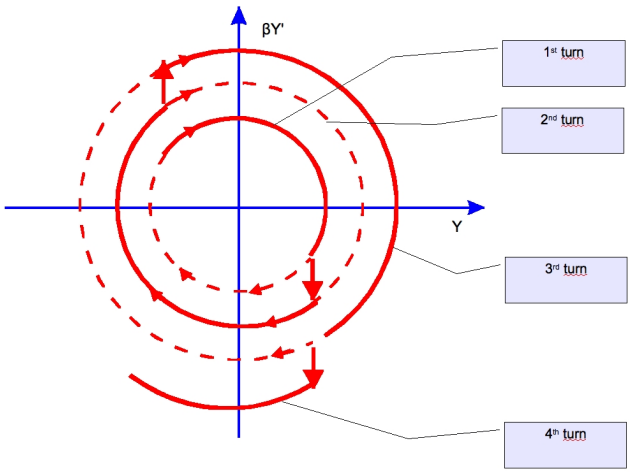

Figure A.3: $\nu_y = 2.5$. Quadrupole effect in the vertical plane if tune is multiple of half integer, known as half-integer resonance.

For example let us take Figure A.3 where is shown, in the transverse vertical phase space (normalized), the effect of a focusing quadrupole with a tune of $\nu_y = 2.5$. At every turn the divergence y' (β is constant) and the position y increase, causing beam loss. This is called a second order or half integer resonance. For sextupoles this is true if the tune is a multiple of 1/3 (third order resonance) and, in general, considering al multipoles, the tunes need to be irrational numbers to avoid this resonances. Any way, higher order resonances are not strong producing effects only after many turns.

If motion is coupled it may be possible to arise also sum and difference betatron resonances. Those are described by:

$$m\nu_x \pm l\nu_y = n$$

where m, l, n are integers with $m, l \neq 0$.

Tune diagrams as in Figure 1.7 may be built to show the best tunes to chose to have a large available working area.

Synchrobetatron resonances

Synchrobetatron resonances are due to coupling between the longitudinal and transverse motion. Those arise when the following relation among the transverse (x,y) and longitudinal (s) tunes ν subsists:

$$m\nu_x + l\nu_y + k\nu_s = n$$

where m, l, k, n are integers with $m, l, k \neq 0$. This resonances reduce lifetime drastically and limit the performance of circular accelerators. The main mechanism for excitation of this resonances are: dispersion in sextupoles, dispersion in RF cavities and beam beam interaction at a crossing angle.

Dipole Kick

The effect of a dipole kick producing a deflection θ on the orbit is the following:

$$y(s_1) = \frac{1}{2}\beta(s_1)\theta(s_1)\cot\pi\nu$$

(where ν is the tune) giving a sinusoidal orbit. The consequent orbit variation expressed in terms of Twiss parameters is

$$y'(s_1) = \frac{1}{2}\theta(s_1)\left[1 - \alpha(s_1)\cot\pi\nu\right]$$

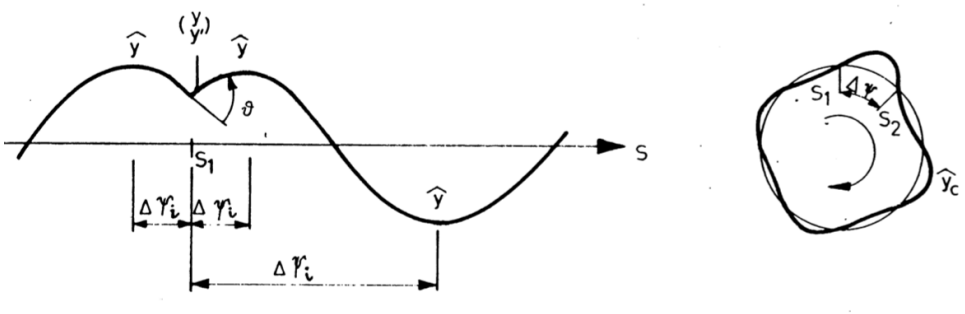

Figure A.4: Dipole kick

Hourglass effect

We may write the luminosity at the IP as

$$\mathcal{L} = \frac{2I^2B}{4\pi e^2 f_0 \epsilon \beta^*}\sqrt{\frac{k'}{k}}H(r, \nu_0, \alpha) \tag{A.1}$$

$$r = \frac{\beta^*}{\sigma_s} \tag{A.2}$$

$$H(r, \nu_0, \alpha) = \cos^2(\alpha)\frac{r}{\sqrt{\pi}}e^{\frac{r^2}{2}(1+\nu_0)}K_0\left[\frac{r^2}{2}(1+\nu_0)\right] \tag{A.3}$$

where H is the hourglass effect, I the beam currents, B the number of bunches and K_0 the modified Bassel function.
Plot of the effect for $\alpha = 0.0025$ and $\nu_0 = 0.065$ is shown in Figure A.5.

Flat Beam hourglass effect

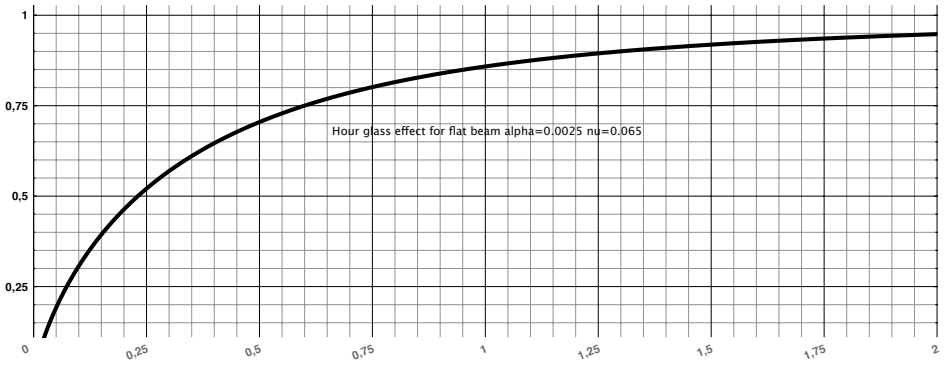

Figure A.5: Hourglass effect in function of $r = \frac{\beta^*}{\sigma_s}$

From this equation it is clear that β_y needs to be not smaller than the bunch length to avoid a luminosity reduction due to hourglass effect while high luminosity is evidently obtained decreasing the bunch length σ_s as it is clear from equation A.1 [49].

More generally, for an asymmetric collider this effect is defined by [50]

$$\frac{\mathcal{L}}{\mathcal{L}_0} = \int_{-\infty}^{+\infty} \frac{dt}{\sqrt{\pi}} \frac{e^{-t^2}}{\sqrt{(1+\frac{t^2}{t_x^2})(1+\frac{t^2}{t_y^2})}} \tag{A.4}$$

$$t_x^2 = \frac{2(\sigma_{x+}^{*2} + \sigma_{x-}^{*2})}{(\sigma_{s+}^2 + \sigma_{s-}^2)(\frac{\sigma_{x+}^{*2}}{\beta_{x+}^{*2}} + \frac{\sigma_{x-}^{*2}}{\beta_{x-}^{*2}})} \tag{A.5}$$

where a similar equation for t_y holds, $+/-$ indicates the energy and the $*$ indicates the IP. These relations confirm in the general case that smaller β for both beams leads necessary to smaller bunch length to avoid the influence of Hourglass effect.

Synchrotron Integrals

Beam parameters in a storage ring are modified by the emission process of synchrotron radiation. These effects are governed by radiation integrals.

$$
\begin{aligned}
I_1[m] &= \oint \left(\frac{D_x}{\rho_x} + \frac{D_y}{\rho_y} \right) ds \\
I_2[m^{-1}] &= \oint \left(\frac{1}{\rho_x^2} + \frac{1}{\rho_y^2} \right) ds \\
I_3[m^{-2}] &= \oint \left(\frac{1}{|\rho_x^3|} + \frac{1}{|\rho_y^3|} \right) ds \\
I_{4x}[m^{-1}] &= \oint \frac{(1-2n)D_x}{\rho^3} ds \\
I_{5x}[m^{-1}] &= \oint \frac{\gamma_x D_x^2 + 2\alpha_x D_x D_x' + \beta_x D_x'^2}{\rho^3} ds,
\end{aligned}
$$

γ is the Lorenz factor. Integrals are taken around the ring, ρ is the local bending radius, D and D′ the local dispersion and dispersion derivative and α and β the Twiss parameters.

Flat beams

For the parameterization of flat beams, we take

$$
\begin{aligned}
\epsilon_x &= \epsilon \\
\epsilon_y &= k\epsilon \\
\beta_y^* &= \beta^* \\
\beta_x^* &= \frac{\beta^*}{k'} \\
\nu_0 &= \frac{\alpha\sigma_s}{\sqrt{\beta_x^*\epsilon}} = \alpha\sigma_s\sqrt{\frac{k'}{\epsilon\beta^*}}
\end{aligned}
$$

where ϵ is the equilibrium emittance, $k << 1$ is the coupling parameter, $k' = \frac{\beta_y^*}{\beta_x^*} << 1$ is the flatness parameter, and α is the half crossing angle.

A.2 CKM

In the Standard Model (SM) there are 3 families of quarks, (u,d), (c,s) and (t,b). While strong interactions occur only within families, conserving flavor, weak interactions may mix flavors. This mixing is described by The Cabbibo-Kobayashi-Maskawa Matrix:

Mixing and CKM

$$V_{CKM} = \begin{pmatrix} V_{ud} & V_{us} & V_{ub} \\ V_{cd} & V_{cs} & V_{cb} \\ V_{td} & V_{ts} & V_{tb} \end{pmatrix}$$

so that

$$\begin{pmatrix} d' \\ s' \\ t' \end{pmatrix} = V_{CKM} \begin{pmatrix} d \\ s \\ t \end{pmatrix}$$

are the eigenstates of weak interactions.
The V_{CKM} matrix has to be a unitary matrix ($VV^\dagger = 1$) due to local gauge invariance and conservation of baryon number. To account for this the following relations need to be true:

$$V_{ud}^* V_{cd} + V_{us}^* V_{cs} + V_{ub}^* V_{cb} = 0 \quad \text{(A.6)}$$
$$V_{ud}^* V_{td} + V_{us}^* V_{ts} + V_{ub}^* V_{tb} = 0 \quad \text{(A.7)}$$
$$V_{cd}^* V_{td} + V_{cs}^* V_{ts} + V_{cb}^* V_{tb} = 0 \quad \text{(A.8)}$$
$$V_{ud} V_{us}^* + V_{cd} V_{cs}^* + V_{td} V_{ts}^* = 0 \quad \text{(A.9)}$$
$$V_{ud} V_{ub}^* + V_{cd} V_{cb}^* + V_{td} V_{tb}^* = 0 \quad \text{(A.10)}$$
$$V_{us} V_{ub}^* + V_{cs} V_{cb}^* + V_{ts} V_{tb}^* = 0. \quad \text{(A.11)}$$

The matrix may be written in the Wolfstein parameterization (third order) as:

$$V_{CKM} = \begin{pmatrix} 1 - \frac{\lambda^2}{2} & \lambda & A\lambda^3(\rho - i\eta + i\eta\frac{\lambda^2}{2}) \\ -\lambda & 1 - \frac{\lambda^2}{2} - i\eta A\lambda^4 & A\lambda^2(1 + i\eta\lambda^2) \\ A\lambda^3(1 - \rho - i\eta) & -A\lambda^2 & 1 \end{pmatrix}$$

where λ,A,ρ and η are the 3 parameters and the phase. The variables λ and A are well known since they are determined by the Cabibbo angle, so the attention is focused on ρ and η. Equations from A.6 to A.11 may be represented in the complex plane in the so called unitarity triangles as in Figure A.6.

This triangle (eq. A.11) is the most appealing among the 6 possible since the sides are of the same order of magnitude λ^3.

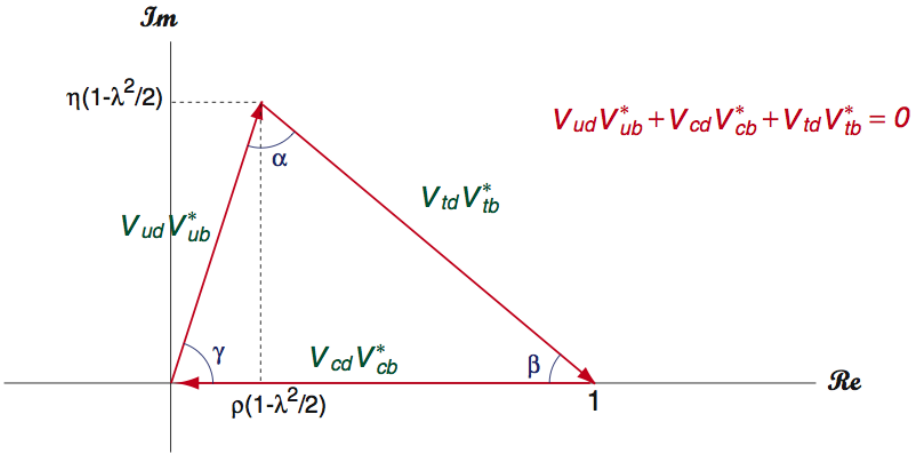

Figure A.6: Unitary Triangle

A.3 TOOL OPERATIONS

Below is a schematic description of the procedure followed by the tool to realize the simulations.

- **Define Input** All the commands for Mad-X are written by Matlab on the input file, reading from the interface the settings to be applied for elements installation, misalignment, number of iterations for simulations and correction parameters. The interface itself triggers same preventive calculations to retrieve information from the sequence loaded as the elements names and their positions. At execution of the *Start* button everything is fixed and the input file is fed to Mad-X.

- **Install Elements** Any element in the sequence may be selected to have a corrector, a monitor or a skew quadrupole installed after it. Matlab, recognizes if there is free available space in the sequence and gives instructions to Mad-X to place the element at the center of that space. A constraint on the minimum amount of free space after the element is also possible to be sure that the space necessary for the real element to be installed is available. This operation is done only for the first simulation and the complete sequence is saved to be used directly in the other simulations. SuperB does not have correctors and monitors installed in its present version, so in the analysis they are all set via the

interface. If the lattice already contains BPM, correctors and skew quadrupoles, they will of course be considered in the simulations.

- **Calculate Matrices** If the calculation of response matrices is required, Matlab adds at the beginning of the input the necessary code to calculate all the orbits and before correction takes place it uses the produced files to build the response matrices that will be used in the simulations. This calculation takes place only once, before misalignments are applied to the lattice.

- **Simulate** It is possible to set simulations for any range of variances, to decide the number of simulation iterations for a single variance and the number of steps to be taken in the given range. For this purpose the code repeats the following procedure changing the seed of misalignments at the beginning of every simulation:

  - **Apply Misalignments** Misalignments are applied to the elements in the machine. The values of the different misalignments for every element are selected from truncated gaussians with the variances determined by the current step within the intervals defined by the user for that particular element and error. To start the correction a first reading of the machine orbits is made with sextupole off.

  - **Apply BPM reading errors** Turn by turn errors are implemented at this stage using Matlab. At every reading given by MadX, Matlab adds a random value distributed as the desired resolution. In the construction of the response matrices, these errors are not taken into account, like all the other imperfections.

  - **Correction re-iteration** For what concerns the Steering parameters the GUI enables a quite flexible interface. Relative weights α and ω may be set independently while keeping the constraint that their sum is at most 1. It is also possible to build a plot to determine the optimum number of eigenvectors setting the starting point and the number of eigenvector to study via the *scan* edit button. The plot obtained may then be seen via the plot interface. The correction parameters are loaded and correction re-iteration is performed according to the settings given by the user following these two steps:

    Steering Settings on the GUI

    * **Apply Correction** Matlab calculates the correction independently in the two planes and rebuilds a new Mad-X input to calculate the effect of the correction.

    * **Read orbits** At the end of every simulation with correction applied all the quantities constrained by the correction are recalculated for reiteration of the procedure. The *twiss* command is used to determine the orbits at the BPM and the *emit* command is used to calculate the emittances.
    * **BPM errors** Turn by turn reading errors are applied again.

    It is also possible to apply a pre-correction of the orbit (reiteration is also possible) with sextupoles off.

  – **Store Results** The last measured parameters are stored in files.

- **Plot Results** The user may now ask for a number of variable to be plotted in the interface. The quantities that may be shown and eventually saved are (in both planes):
  – emittance
  – rms orbit
  – rms dispersion
  – orbit at monitors
  – dispersion at monitors
  – measured coupling at monitors
  – measured beating at monitors
  – measured coupling at monitors
  – response matrices
  – applied misalignments
  – relative difference from design dispersion
  – maximum dispersion
  – rms coupling
  – rms β-beating ($\frac{\beta_u - \beta_{uD}}{\beta_{uD}}$)
  – β-beating
  – square sum of coupling matrix elements

  All these quantities, except for matrices, are shown before and after correction. The tool automatically selects the best kind of plot according to the number of steps selected for the simulations. In the case of a single variance histograms of the of the wished parameter are plotted. While, for multiple steps, plots like those presented for the correction scheme comparison in chapter 2 are produced, where the dot is the average of the distribution, and the

error bars represent the 5th and 95th percentile of the distribution obtained for that particular set of misalignment variances.

More tool capabilities

The tool developed has also other capabilities developed under the influence of parallel activities. These are:

- Convert sequence of misaligned elements to SLIM compatible format, and convert SLIM to MADX
- Draw view of sequence as parallelepipeds of different colors (one for every element)
- Plot from previously saved file

BIBLIOGRAPHY

[1] PEP II conceptual design report. Technical report, SLAC-372, LBL-PUB-5303, CALT-68-1715, UCRL-ID-106426, UC-IIRPA-91-01, 1991. (Cited on page 4.)

[2] S. Kurokawa and E. Kikutani. Overviw of the KEKB accelerators. *Nuclear Instruments and Methods in Physics Research A*, 499(1), 2003. (Cited on page 4.)

[3] M. Zobov et al. Test of "crab-waist" collisions at the DAΦNE Φ factory. *Phys. Rev. Lett.*, 104(17):174801, Apr 2010. (Cited on pages 4 and 18.)

[4] Cyrille Thomas, Guenther Rehm, Ian Martin, and Riccardo Bartolini. X-ray pinhole camera resolution and emittance measurement. *Phys. Rev. ST Accel. Beams*, 13(2):022805, Feb 2010. (Cited on page 4.)

[5] Andreas Luedeke, Ake Andersson, Michael Böge, Babak Kalantari, Boris Keil, Marco Pedrozzi, Thomas Schilcher, Volker Schlott, and Andreas Streun. Status of the Swiss Light Source. page 3 p, 2006. (Cited on page 4.)

[6] CERN SL/93-19 (DI) J. Poole, ed., editor. *Proceedings of the third Workshop on LEP Performance*. (Cited on page 5.)

[7] SuperB Collaboration. SuperB: A high-luminosity asymmetric e+ e- super flavor factory. Conceptual Design Report, 2007. (Cited on page 7.)

[8] SuperB Collaboration. SuperB: A high-luminosity asymmetric e^+e^- super flavor factory. Technical Design Report, not yet published (2010). (Cited on page 7.)

[9] M.Rama. The SuperB project. *Il Nuovo Cimento*, (not yet published). (Cited on pages 7 and 8.)

[10] D. Griffiths. *Introduction to Elementary Particles*. John Wiley & Sons, New York, USA, 1987. (Cited on page 7.)

[11] N. Harnew et al. The physics performance of LHCb. In Nucl. Instrum. Meth., editor, *5th International Workshop on Physics in Hadron Machines (Beauty 97), Santa Monica.*, volume A 408, 1998. (Cited on page 7.)

[12] B. Aubert et al. Time-dependent and time-integrated angular analysis of $B \to \varphi K^0_S \pi^0$ and $\varphi K^{\pm}\pi^{\mp}$. *Nuclear Instruments and Methods in Physics Research A*, 479(1), 2002. (Cited on page 8.)

[13] A. Abashian et al. Improved search for D^0-$\bar{D}^0$ mixing using semileptonic decays at Belle. *Nuclear Instruments and Methods in Physics Research A*, 479(117), 2002. (Cited on page 8.)

[14] BABAR Collaboration. Measurement of time-dependent CP asymmetries in $B_0 - > K^0_S K^0_S K^0_S$ decay. *arXiv:hep-ex/0607108v1*. (Cited on page 9.)

[15] C. Bozzi et al. The BABAR silicon vertex tracker. *Nuclear Instruments and Methods in Physics Research Section A: Accelerators, Spectrometers, Detectors and Associated Equipment*, 453(1-2):78 – 83, 2000. (Cited on page 9.)

[16] M. Zabov. Beam-beam interaction in novel, very high luminosity parameter regimes. In *Proceedings of IPAC 2010*, 2010. (Cited on page 13.)

[17] V.V.Danilov et al. The concept of round colliding beams. In *Proceedings of EPAC96*, 1996. (Cited on pages 14 and 15.)

[18] R.B.Palmer. Energy scaling, crab crossing and the pair problem. *SLAC-PUB-4707*, 1988. (Cited on page 16.)

[19] Katsunobu Oide and Kaoru Yokoya. Beam-beam collision scheme for storage-ring colliders. *Phys. Rev. A*, 40(1):315–316, Jul 1989. (Cited on page 16.)

[20] Kohji Hirata. Analysis of Beam-Beam Interactions with a Large Crossing Angle. *Phys. Rev. Lett.*, 74(12):2228–2231, Mar 1995. (Cited on page 16.)

[21] A. Gallo et al. Strong RF focusing for luminosity increase: short bunches at IP. *SLAC-PUB-10409*, October 2003. (Cited on page 16.)

[22] Y.Onishi. *ICFA Beam Dynamics Newsletter 48:252*, 2009. (Cited on page 16.)

[23] Pantaleo Raimondi. in 2nd SuperB Workshop. 2006. (Cited on page 16.)

[24] Pantaleo Raimondi et al. Beam-beam issues for colliding schemes with large Piwinski angle and crabbed waist. *LNF-07/003 (IR)*, 2007. (Cited on page 16.)

[25] D. Shatilov and M. Zabov. *ICFA Beam Dynamics Newsletter*, (37):99, 2005. (Cited on page 16.)

[26] Helmut Wiedemann. *Particle Accelerator Physics*. Springer, third edition, 2007. (Cited on pages 18, 69, 70, and 71.)

[27] Dimitry Shatilov. Example of x-y resonance supression. ICFA08 Workshop. (Cited on page 18.)

[28] J. Guo et al. Low emittance e^+e^- storage ring design using bending magnets with longitudinal gradient. SLAC internal Publication. (Cited on page 20.)

[29] S.Y.Lee. *Accelerator Physics*. World Scientific, 1999. (Cited on page 20.)

[30] Vic Suller. Synchrotron radiation sources past, present and future. CAMD Louisiana and SRS Daresbury. (Cited on page 21.)

[31] Y.Nosochkov et al. Super-B lattice studies. In *Proceedings of IPAC 2010*, 2010. (Cited on page 22.)

[32] M.Biagini et al. The Super-B project accelerator status. In *Proceedings of IPAC 2010*, 2010. (Cited on page 22.)

[33] R.V. Servranckx and K.L. Brown. Chromatic correction for large storage rings. *IEEE Trans. NS-26,3598*, 1979. (Cited on page 25.)

[34] V. Balakin et al. Focusing of submicron beams for TeV scale e^+e^- linear colliders. *Phys. Rev. Lett.*, 74:2479–2482, 1995. (Cited on page 26.)

[35] Y. Honda et al. Measurements of electron beam emittance in the accelerator test facility damping ring operated in multibunch modes. *Phys. Rev. ST Accel. Beams*, 6:092802, 2003. (Cited on page 26.)

[36] K. Kubo et al. Extremely low vertical emittance beam in accelerator test facility at KEK. *Phys. Rev. Lett.*, 88:194801, 2002. (Cited on page 26.)

[37] Pantaleo Raimondi and Andrei Seryi. A novel final focus design for future linear colliders. *Phys. Rev. Lett.*, 86:3779–3782, 2001. (Cited on page 26.)

[38] E Paoloni, S Bettoni, M E Biagini, and P Raimondi. Magnetic design studies for the final focus quadrupoles of the SuperB large crossing angle collision scheme. page 3 p, 2008. (Cited on page 26.)

[39] Bryan W. Montague. Polarized beams in high energy storage rings. *Physics Reports*, 113(1):1 – 96, 1984. (Cited on page 27.)

[40] R. Assmann, P. Raimondi, G. Roy, and J. Wenninger. Emittance optimization with dispersion free steering at LEP. *Phys. Rev. ST Accel. Beams*, 3(12):121001, Dec 2000. (Cited on page 37.)

[41] Lloyd Trefethen. *Numerical Linear Algebra*. Peachpit Press, Berkeley, 1997. (Cited on page 38.)

[42] L S Nadolski. Use of LOCO at synchrotron SOLEIL. page 3 p, 2008. (Cited on page 39.)

[43] MAD-X Home Page. http://mad.web.cern.ch/mad/. (Cited on page 48.)

[44] MATLAB. version 7.4. *Natick, Massachusetts: The MathWorks Inc.*, 2007. (Cited on page 48.)

[45] M.H. Donald. private comunication. (Cited on page 51.)

[46] K. Panagiotidis. Alignment sensitivities in the ILC damping rings. In *Proceedings of PAC07*, Albuquerque, New Mexico, USA, 2007. (Cited on page 51.)

[47] Georg H. Hoffstaetter et al. Orbit-response matrix analysis at hera. In *EPAC'02*. DESY, Hamburg, Germany, 2002. (Cited on page 64.)

[48] A.W. Chao and M. Tigner. *Handbook of accelerator physics and engineering*. World Scientific, 1998. (Cited on page 69.)

[49] G.Dugan. Dependence of luminosity in CESR on bunch length for flat and round beams. *Laboratory of Nuclear Studies, Cornell University, Ithaca, NY 14853*, (CBN96-15). (Cited on page 74.)

[50] M.A. Furman. Hourglass effect for asymmetric colliders, May 1999. (Cited on page 74.)